

Stromal cell Protein kinase C- β inhibition enhances chemosensitivity in B cell malignancies and overcomes drug resistance

Eugene Park^{1‡}, Jingyu Chen^{1‡}, Andrew Moore^{1‡}, Maurizio Mangolini¹, Antonella Santoro¹, Joseph R. Boyd², Hilde Schjerven^{3,4}, Veronika Ecker^{5,6}, Maike Buchner^{5,6}, James C. Williamson⁷, Paul J. Lehner⁷, Luca Gasparoli⁸, Owen Williams⁸, Johannes Bloehdorn⁹, Stephan Stilgenbauer⁹, Michael Leitges¹⁰, Alexander Egle^{11,12,13}, Marc Schmidt-Supprian^{14,15}, Seth Frieze¹⁶ and Ingo Ringshausen¹

‡ equal contribution

1. Wellcome Trust/ MRC Cambridge Stem Cell Institute & Department of Haematology, University of Cambridge, Cambridge CB2 0AH, United Kingdom.
2. Department of Biochemistry and University of Vermont Cancer Center, The University of Vermont Larner College of Medicine, Burlington, 05405 Vermont, USA.
3. Department of Laboratory Medicine, University of California, San Francisco (UCSF), San Francisco, CA 94143, USA.
4. KG Jebsen Centre for B cell Malignancies, OUH, 0425-Oslo, Norway.
5. Institut für Klinische Chemie und Pathobiochemie, Klinikum rechts der Isar, Technische Universität München, 81675 Munich, Germany.
6. TranslaTUM, Center for Translational Cancer Research, Technische Universität München, 81675 Munich, Germany.
7. Cambridge Institute for Medical Research (CIMR), University of Cambridge, Cambridge, CB2 0XY, United Kingdom.
8. University College London (UCL) GOS-ICH, London WC1N 1EH, United Kingdom.
9. Department of Internal Medicine III, University of Ulm, 89081 Ulm, Germany.
10. PKC Research Consult, Hofstrasse 31, 51061 Cologne, Germany.
11. IIIrd Medical Department with Hematology, Medical Oncology, Hemostaseology, Infectious Diseases and Rheumatology, Oncologic Center; Paracelsus Medical University Salzburg, Cancer Cluster 5020 Salzburg, Austria.
12. Salzburg Cancer Research Institute (SCRI) with Laboratory of Immunological and Molecular Cancer Research (LIMCR), 5020 Salzburg, Austria.
13. Cancer Cluster Salzburg, 5020 Salzburg, Austria.
14. German Cancer Consortium, DKFZ, 69120 Heidelberg, Germany.
15. Department of Haematology, Technical University, 81675 Munich, Germany.
16. Department Biomedical and Health Sciences, University of Vermont, 05405 Burlington, Vermont, USA

Abstract word count: 149

Corresponding author:

Ingo Ringshausen M.D.

University of Cambridge
Wellcome Trust/ MRC Cambridge Stem Cell Institute & Department of Haematology
Jeffrey Cheah Biomedical Centre
Cambridge Biomedical Campus
Puddicombe Way
CB2 0AW Cambridge
United Kingdom
Phone: +44 1223 762086
Email: ir279@cam.ac.uk

ABSTRACT

Overcoming drug-resistance remains a key challenge to cure patients with acute and chronic B cell malignancies. Here we describe a stroma cell autonomous signaling pathway, which contributes to drug resistance of malignant B cells. We show that protein kinase C (PKC)- β -dependent signals from bone marrow derived stroma cells markedly decrease the efficacy of cytotoxic therapies. Conversely, small molecule PKC- β inhibitors antagonize pro-survival signals from stroma cells and sensitize tumor cells to targeted and non-targeted chemotherapy, leading to enhanced cytotoxicity and prolonged survival *in vivo*. Mechanistically, stromal PKC- β controls the expression of adhesion- and matrix proteins, required for **Phosphoinositide 3-kinases (PI3K) activation** and the ERK-mediated stabilization of BCL-X_L in tumor cells. Central to the stroma-mediated drug resistance is the PKC- β dependent activation of transcription factor EB (TFEB), regulating lysosome biogenesis and plasma membrane integrity. Stroma directed therapies, enabled by direct inhibition of PKC- β , enhance the effectiveness of many anti-leukemic therapies.

SUMMARY

Inhibition of stroma cell PKC- β mitigates environment-mediated drug resistance in B cell malignancies.

INTRODUCTION

Over the past decade next generation sequencing technologies provided opportunities to comprehensively describe the spectrum of genomic abnormalities found in various different B cell malignancies(1-4). Ultimately, this has improved our understanding of the underlying genetic mutations contributing to uncontrolled proliferation and extended cell survival while enabling the development of targeted therapies. Notably, drug resistance remains one of the most challenging clinical problems, reflected by the invariable disease recurrence of all low-grade lymphoma-, chronic lymphocytic leukemia (CLL) patients and a substantial fraction of patients suffering from acute lymphoblastic leukemia and high-grade lymphoma. Thus, although a majority of patients achieve disease remissions, relapses occur from cells surviving cancer-therapies. Identifying and targeting cells, which have acquired properties to survive these treatments may ultimately allow to fully eradicate these tumor cells and to achieve cure.

It has been recognized for some time that the tumor microenvironment plays a pivotal role for drug resistance by providing protective niches for tumor cells(5), allowing them to survive targeted and non-targeted therapies through the provision of anti-apoptotic signals. The bone marrow microenvironment appears to be of crucial importance for lymphoid diseases as minimal-residual disease detected in this compartment has a strong prognostic power to predict disease relapse in acute and chronic leukemia and lymphomas(6, 7). Several intermediates of the bone marrow microenvironment to tumor cell communications have been identified, but their targeting has been proven to be difficult and to result in minor effects at best (8),(9).

Here we describe a stroma cell autonomous signaling pathway, dependent on the expression and activation of protein kinase C- β (PKC- β) and subsequent activation of the transcription factor EB, both being of key importance to protect malignant B cells from cytotoxic therapies. Importantly, the dependency of malignant B cells on PKC- β -activity in the microenvironment can be therapeutically exploited with small molecule inhibitors, to treat patients with different B cell malignancies, including CLL, mantle cell lymphoma (MCL) and B cell acute lymphoblastic leukemia (B-ALL).

RESULTS

Stroma PKC- β is essential for survival, but not homing or proliferation of TCL1-tg B cell tumors

Our previous data demonstrated that PKC- β activity in **mesenchymal stroma cells (MSC)** is essential for the engraftment of malignant B cells derived from *E μ -TCL1-tg* mice(10), a model resembling human CLL(11). To further investigate the mechanisms underlying this phenotype, our experiments set out to characterize the role of stromal PKC- β for tumor cell homing, proliferation and survival. Carboxyfluorescein-succinimidyl-ester(CFSE)- labeled CD5⁺CD19⁺ tumor cells from diseased *TCL1-tg* mice were transplanted intravenously (i.v.) and intraperitoneal (i.p.) into either PKC- β knock out (KO) or wild-type (WT) recipient mice. In addition, malignant cells were transplanted into WT mice, which were pre-treated for 48 hours with the PKC- β -inhibitor enzastaurin (60 mg/kg BID) or vehicle control and continued to receive treatment for 48 hours post-transplantation (fig. S1A). Tumor cells homed to the spleen and bone marrow of all recipient mice, irrespectively of PKC- β expression in the microenvironment or its pharmacological inhibition (fig. S1, B and C). A separate cohort of PKC- β KO and WT recipient mice was followed for 2 weeks and tumor engraftment was assessed in the peripheral blood, lymphatic tissues and the peritoneal cavity. A similar number of CFSE-labeled tumor cells were detectable in the peripheral blood of KO and WT mice on day 2. However, from day 8 onwards, we observed a marked increase of tumor cells in the peripheral blood of WT, but not in KO mice (fig. S1D). Two weeks after transplantation of tumor cells, malignant B cells were virtually absent in the bone marrow of KO mice and decreased in the spleen and peritoneal cavity of KO mice, in contrast to WT control mice where tumor cells were maintained (Fig. 1A and fig. S1E). **During the first 2 weeks, disease progression was more pronounced in the bone marrow, which showed a stronger dependency on PKC- β compared to spleen or peritoneal cavity (Fig. 1B).** The continuous decay of the CFSE-label with each cell division did not differ in KO and WT recipient mice (Fig. 1, C and D), **indicating that PKC- β expression in the tumor microenvironment is dispensable for tumor cell homing or proliferation but required to provide pro-survival factors, essential for engraftment and disease progression.**

PKC- β expression in stroma cells is essential for tumor cell engraftment and normal B1 cell development

We were then interested in investigating whether the lack of tumor cell engraftment in PKC- β KO mice was entirely attributed to its absence in stroma cells or whether hematopoietic cells in the microenvironment also contributed. **Germ-line deletion of PKC- β in mice causes**

immunodeficiency with a marked reduction of peritoneal B1 cells and a reduction in serum IgM and IgG3(12). Notably, no differences of white blood cells (WBC), hemoglobin or platelets were observed between WT and KO cells (fig. S2, A and B), also reflected by the presence of similar numbers of Lin⁻Sca1⁺C-Kit⁺ (LSK) and CD45⁺EPCR⁺CD150⁺CD48⁻ (ESLAM) hematopoietic stem cells in the bone marrow (fig. S2C). In addition, the development of normal B cells was not affected by the germ-line deletion of PKC- β , with B-cell progenitor fractions (Hardy fractions A-D(13)) statistically similar between genotypes for both the frequency and absolute number of cells present per femur (fig. S2, D to F).

By generating mixed chimeras, differing only in the expression of PKC- β in the hematopoietic system, we could address whether the engraftment-dependence on microenvironment PKC- β signals is due to the malignant transformation or reflects properties of the cell-of-origin. The cell-of-origin is thought to be a CD5⁺ B cell(14), in mouse most likely a CD5⁺ B1 cell, an innate type of B cell responsible for the production of natural antibodies. We generated PKC- β chimeric mice by transplanting PKC- β WT CD45⁺ hematopoietic bone marrow cells into lethally irradiated (10 Gy) KO animals. To allow for the assessment of chimerism WT CD45.1⁺ bone marrow cells were transplanted into CD45.2⁺ KO recipient mice. As controls, KO CD45.2⁺ BM cells were transplanted into CD45.1⁺ WT recipient mice (Fig. 1E and fig. S3A). Strikingly, in BM-reconstituted WT recipient animals we found no difference in the number of peritoneal B1 cells derived from either PKC- β KO or WT donor cells. Conversely, the development of peritoneal B1 cells in KO recipient animals transplanted from WT bone marrow was significantly ($p=0.02$) reduced compared to WT recipient animals. Notably, the number of peritoneal B1 cells was still higher in these mice than in PKC- β KO control recipients reconstituted with KO bone marrow (Fig. 1F and fig. S3B). Analogous to the germ-line deletion of PKC- β , reconstitution of WT bone marrow in KO recipients was associated with reduced serum titers of the natural antibodies IgM and IgG3, whereas KO cells produced equivalent amounts of antibodies as WT cells in a WT background (Fig. 1G). These data demonstrate that PKC- β is an important cell-extrinsic factor for B cell development. To assess whether the differences in serum IgM and IgG3 titers were further associated with a PKC- β -dependent skewing of plasma cell differentiation, we compared chimerism of donor CD45⁺, CD138⁺ to donor CD45⁺, CD138⁻ cells in the bone marrow and spleen. We found similar engraftment of either genotype in the bone marrow of PKC- β WT and KO recipient animals with no differences between CD138⁺ and CD138⁻ cells (fig. S3, D and E). PKC- β WT donor cells also differentiated equally well in the spleens of either WT or KO recipient animals, whereas PKC- β KO donor cells gave rise to fewer splenic CD45⁺ CD138⁺ cells in a WT background (fig. S3, D and F).

To address whether PKC- β expressed in hematopoietic cells could rescue tumor cell survival in PKC- β KO recipient animals, we injected *TCL1*-tumor cells into KO animals, previously transplanted with KO or WT CD45⁺ bone marrow cells (Fig. 1H). All recipient chimeric mice were deficient for PKC- β in non-hematopoietic cells, but either did (WT \rightarrow KO) or did not (KO \rightarrow KO) contain PKC- β -expressing hematopoietic cells. Similar to our transplantation studies into non-chimeric mice, engraftment of tumor cells in the peripheral blood of WT \rightarrow KO animals compared to WT control mice was significantly ($p=0.001$) impaired (Fig. 1I and J). On the other hand, WT \rightarrow KO recipients contained only slightly more malignant cells than KO \rightarrow KO recipients, indicating that PKC- β -mediated survival signals by non-hematopoietic cells play a predominant role in tumor maintenance.

Inhibition of stromal PKC- β mitigates environment-mediated drug resistance

Signals derived from the microenvironment contribute not only to the development of normal hematopoietic cells, but also to drug resistance of malignant cells (termed environment-mediated drug resistance; EMDR)(5). The marked dependency of malignant B cell survival on PKC- β activity in the microenvironment raised the possibility that this interaction could be exploited therapeutically. To test this hypothesis, we cultured primary human CLL cells on bone marrow derived MSCs from either KO or WT mice. Notably, human MSCs were indistinguishable from mouse MSCs with regard to PKC- β activation and survival support(10). In line with our previous observations, PKC- β deficiency in bone marrow derived MSCs mitigated the anti-apoptotic effects of stromal cells on CLL cells (Fig. 2, A and B). To test the role of stromal PKC- β in EMDR, parallel co-cultures were exposed 24 hours post-CLL seeding to increasing doses of venetoclax (BCL2-inhibitor), bendamustine (alkylating agent), fludarabine (purine analogue) or ibrutinib and idelalisib, (inhibitors of B-cell receptor (BCR) - induced kinases), before assessing the viability of CLL cells 48 hours later. Expectedly, contact with WT MSCs enhanced the resistance of CLL cells to these cytotoxic drugs when compared to suspension cells in mono-culture (Fig. 2C). In particular, we observed strong protective effects of MSCs on CLL cells for venetoclax and fludarabine-treatments, while EMDR to BCR-inhibitors was less pronounced. The absence of PKC- β in MSCs completely abolished the protective effects seen with WT stromal cells under all treatments except for bendamustine, where PKC- β -deficiency nevertheless also strongly decreased stroma protection. Notably, PKC- β expression in monocytes, which are derived from the hematopoietic system and also support leukemogenesis(15), was dispensable for response to cytotoxic therapies (fig. S4, A to D). These data indicate that PKC- β expression in MSCs is crucial for EMDR of primary CLL cells.

We previously demonstrated that PKC- β kinase activity in MSCs is essential for microenvironment-mediated survival support of leukemia cells(10). Therefore, we tested whether ablation of EMDR could be achieved with small molecule PKC-inhibitors. Enzastaurin and sotrastaurin are orally bioavailable, reversible ATP-competitive inhibitors of PKCs with **enzastaurin being more specific for the β -isoform** (16, 17). Midostaurin is a multi-kinase inhibitor with activity against PKC-isoforms and was recently approved for the treatment of FLT3-ITD⁺ AML(18). Co-cultures of WT MSCs and primary CLL cells were exposed to increasing low-doses of these inhibitors for 48 hours. Similar to co-culturing CLL cells on KO MSCs, each PKC-inhibitor reduced the viability of CLL cells (Fig. 2D). Importantly, the cytotoxic effects of enzastaurin and sotrastaurin did not exceed the survival-disadvantage of KO MSCs and were dose-dependent, whereas midostaurin induced CLL cell death beyond this effect similarly across all doses. This suggests that midostaurin also inhibits other kinases in MSCs and/or has direct cytotoxic effects on primary CLL cells. To test whether PKC- β inhibitors can sensitize malignant B cells to cytotoxic agents, we treated MSC/CLL-co-cultures for 48 hours with low dose (5 μ M) enzastaurin and increasing doses of different cytotoxic agents. Assessment of apoptotic CLL cells after 48 hours in co-culture indicated that enzastaurin sensitized CLL cells to venetoclax, bendamustine and fludarabine, pheno-copying the experiments with KO stromal cells (Fig. 2E; fig. S4, E and F; patient characteristics are provided in table S1), but not consistently to ibrutinib and idelalisib (fig. S4F). Using the Combenefit platform(19) for the assessment of drug-synergy, the Bliss-independence and the Loewe-additivity models demonstrated that the cytotoxic effects of combinational treatments with venetoclax and PKC- β -inhibitors were indeed synergistic (Fig. 2G and fig. S4G). Similar to enzastaurin, the PKC-inhibitors sotrastaurin and midostaurin also chemo-sensitized malignant B cells to cytotoxic agents (Fig. 2G), indicating a class-rather than a drug-specific effect.

Notably, PKC- β expression is not restricted to MSCs, but also found at high amounts in malignant B cells(20). To prove that the synergistic effects are indeed mediated by the inhibition of stromal PKC- β and not attributed to off-target effects or inhibition of PKC- β expressed in tumor cells, we cultured primary CLL cells on PKC- β KO stromal cells and then exposed co-cultures to enzastaurin in the absence or presence of venetoclax. Analyses of apoptotic B cells after 48 hours demonstrated that enzastaurin did not affect the survival of CLL cells cultured on PKC- β KO stromal cells. Furthermore, under these conditions enzastaurin also did not enhance the cytotoxic effects of venetoclax (Fig. 2F). In conclusion, by genetically removing the target protein for the kinase inhibitor, these data prove that the PKC- β inhibitor sensitizes malignant B cells to cytotoxic drugs by ablating microenvironment-mediated, PKC- β -dependent survival signals and drug resistance.

The chemo-sensitizing effects of enzastaurin were most pronounced in combination with venetoclax. The efficacy of this BCL-2 inhibitor is largely dependent on the relative expression of other anti-apoptotic proteins. To understand how stromal PKC- β inhibits the cytotoxicity of venetoclax, we analyzed the expression of anti-apoptotic proteins in CLL cells cultured either on WT or KO stromal cells. In CLL cells cultured on WT stromal cells and treated with a low-dose of venetoclax, BCL-X_L was significantly ($p=0.009$ at 48 hours post-treatment) up-regulated, whereas expression of BCL2, BCL2A1 and MCL-1 decreased after 48 hours. In contrast to WT stromal cells, the enhanced expression of BCL-X_L was markedly mitigated in CLL cells cultured on KO stromal cells (Fig. 2H, for protein-quantification see fig. S5A). Similar to co-culture on KO stromal cells, treatment of WT stroma-CLL co-cultures with venetoclax or other chemotherapies in combination with enzastaurin also blocked the up-regulation of BCL-X_L in CLL cells (Fig. 2I). Notably, the stroma-dependent stabilization of BCL-X_L was not regulated by enhanced transcription as BCL-X_L transcripts were readily detectable in co-cultured CLL cells and remained stable following venetoclax treatment (fig. S5, B and C). In conclusion, the activation of PKC- β in the microenvironment contributes to drug resistance by controlling the post-transcriptional regulation of BCL-X_L in malignant B cells.

Stromal PKC- β is essential for ERK-activation and BCL-X_L stabilization in CLL cells

To further understand the role of stromal PKC- β in EMDR, RNA-seq expression profiling was performed on primary CLL cells cultured on either WT or KO stroma in the presence of venetoclax (used at a minimal concentration of 1.25 nM to avoid substantial cell death (see Fig. 2C)). Clustering of the global expression changes between conditions demonstrate a considerable difference in the CLL response to venetoclax when co-cultured with WT versus KO stroma (Fig. 3A). Pairwise comparison of gene expression in CLL cells cultured on either WT or KO stroma in the presence of venetoclax identified 810 differentially expressed genes (DEG); of these, 755 were significantly up-regulated in CLL cells cultured on WT stroma compared to cells co-cultured on KO stroma, while 55 genes were down-regulated (adjusted p -value <0.01 ; \log_2 fold-change >1). Gene set enrichment analysis indicates that co-culture on WT stromal cells enhanced the expression of genes required for ECM-remodeling and cell-cell interactions (Fig. 3B and data file S1). We then used Ingenuity Pathway Analysis (IPA) to identify canonical pathways and regulators operating up-stream of these transcriptional changes. These analyses indicated that PI3K and MAPK signaling was inhibited in CLL cells cultured on KO stroma (Fig. 3C) associated with effects on integrin- and TGF- β pathways (fig. S6A). Indeed, immunoblot analysis showed ERK-, but not p38- or JNK-pathway activation in CLL cells cultured on WT stroma under venetoclax exposure.

This activation was severely mitigated in venetoclax-treated tumor cells cultured on KO stromal cells (Fig. 3D, fig. S6B) or cultured on WT stroma in the presence of enzastaurin (fig. S6C). Notably, ERK-activation was associated with enhanced BCL-X_L expression, suggesting a functional link between the two. Indeed, the MEK1/2-inhibitor Trametinib antagonized venetoclax induced ERK-activation, and was associated with decreased BCL-X_L protein expression (Fig. 3E) and enhanced cytotoxicity (Fig. 3F).

Since activation of PI3K has been shown to limit the efficacy of venetoclax (21, 22), we investigated whether the PI3K inhibitor idelalisib also synergized with venetoclax in inducing apoptosis in CLL cells. Indeed, in combination with the PI3K inhibitor, venetoclax-induced apoptosis was enhanced (Fig. 3G) and AKT-phosphorylation, used as a surrogate to assess PI3K activity in malignant B cells, was abolished (Fig. 3H). To distinguish between idelalisib-effects in tumor or stroma cells, we performed immunoblotting from CLL cells cultured in the presence of venetoclax on either WT or KO stroma cells. Results from this experiment indicated that PI3K is activated in venetoclax treated tumor cells and that stroma PKC- β activity contributes to this activation, though this dependency was less pronounced than effects observed on MAPK-signaling (Fig. 3I and fig. S6D).

To provide further evidence that the up-regulation of PKC- β -mediated and EMDR-associated genes has clinical relevance, we retrospectively assessed the impact of stroma-mediated, de-regulated pathways on progression-free and overall survival in a cohort of fludarabine-refractory CLL patients(23). Co-expression of genes in CLL, regulated by stroma PKC- β , was found as a signature in a majority of the drug-resistant cohort (Fig. 3J). Moreover, patients with high co-expression signatures demonstrated a worse prognosis to salvage treatment, compared to low-expression signature patients (Fig. 3K and fig. S6E), emphasizing the relevance of these genes, identified in co-culture, to clinical observations. Conclusively, our *in vitro* data show that stroma-mediated drug resistance to venetoclax is mediated by ERK- and PI3K-signaling, dependent on PKC- β activity in stromal cells.

PKC- β dependent lysosome biogenesis is required for EMDR of B cells

These results prompted us to also investigate the molecular events orchestrated by PKC- β in stromal cells. RNA sequencing analysis was performed using PKC- β WT and KO stromal cells co-cultured with primary CLL cells for 48 hours. A total of 3,352 genes with significantly changed expression (fold-change >2; adjusted p-value <0.05) were identified in PKC- β KO cells, compared with WT cells (Fig. 4A). This demonstrates a broad impact of PKC- β on stromal cell characteristics, including stark differences in the expression of genes encoding plasma membrane- and intracellular vesicular proteins. Nearly half of all annotated plasma

membrane and intracellular vesicular protein genes were differentially regulated between PKC- β WT and KO stroma, with 438 and 287 genes exhibiting greater than a two-fold change in either gene set, respectively (adjusted p-value <0.05). Gene set enrichment analysis (GSEA) revealed PKC- β WT stromal enrichment of genes involved in ECM interactions and lysosome vesicle biogenesis (Fig. 4, B and C). Analysis of lysosome biogenesis by lysosome staining showed a substantially reduced lysosomal content in PKC- β KO cells compared to WT stroma (fig. S7A). Moreover, PKC- β KO stroma was also resistant to chloroquine-induced lysosome accumulation compared to WT stroma. In line with our observations, lysosome biogenesis in osteoclasts has been shown to be controlled by PKC- β mediated serine phosphorylation of the transcription factor EB (TFEB) C-terminal motif(24). Phosphorylation of TFEB increased its nuclear abundance and enhanced transcriptional activity (25).

TFEB is a member of the MiT-TFE family of transcription factors, which are major factors regulating lysosome biogenesis and autophagy (26). To ascertain whether lysosome deregulation extended to stroma in co-culture with CLL under stress conditions, immunoblots for lysosome component protein, LAMP-1, and lysosome biogenesis transcription factor, TFEB, were conducted. Immunoblots showed markedly increased LAMP1 and TFEB protein expression in WT stroma at 24 and 48 hours, respectively, as compared to KO stroma in similarly treated CLL co-cultures (Fig. 4D). Further analysis found increased nuclear expression of TFEB in co-cultured PKC- β WT compared to KO stroma (Fig. 4E and fig. S7B). **To assess the importance of TFEB for stroma-mediated drug resistance, we generated TFEB deficient cells using CRISPR/Cas9 deletion (Fig. 4F). While TFEB deficient stroma cells and control counterparts provided equal survival support for primary CLL cells in the absence of drugs, exposure of co-cultures to venetoclax demonstrated that TFEB is an essential factor for EMDR (Fig. 4G). We used chloroquine and bafilomycin to interrogate whether the inhibition of lysosome function equally inhibits EMDR. Chloroquine-treated co-cultures did not show impaired survival of malignant B cells in contrast to bafilomycin, which reduced the anti-apoptotic effects from stroma on CLL cells. However, both compounds markedly enhanced the cytotoxic effects of venetoclax (Fig. 4H). To disentangle direct inhibitory effects of chloroquine and bafilomycin on CLL and stroma cells, stroma cells were pre-treated with both compounds before their washout, preceding primary CLL co-culture and subsequent venetoclax exposure. Pre-treatment of stroma cells similarly mitigated EMDR, indicating that the synergistic effects were attributed to the inhibition of stroma- and not CLL-lysosomes (fig. S7C). Lastly, complementary to the deletion of TFEB from stroma cells, parental KO stroma cells were transduced with a constitutively-active TFEB variant (caTFEB)(27) or vector control. CLL co-cultured with PKC-**

β KO stroma expressing caTFEB demonstrated a significantly ($p=3.71E-07$) higher resistance to venetoclax compared to cells cultured on control stroma (Fig. 4I and fig. S7D). Additionally, venetoclax exposed CLL cells, co-cultured on PKC- β KO stroma expressing caTFEB, demonstrated increased amounts of BCL-X_L and increased ERK-phosphorylation compared to CLL cells co-cultured on control KO stroma (Fig. 4J). To ascertain whether PKC- β inhibition impairs *in vivo* lysosomal biogenesis, *TCL1*-transplanted recipient mice were treated with enzastaurin. **Stroma**-restricted down-regulation of both lysosomal-associated membrane protein (LAMP)-1 and LAMP-2 was observed in the enzastaurin co-treated cohort, in comparison to venetoclax-treated and vehicle control cohorts, respectively (Fig. 4K). In contrast, these lysosome-associated proteins were unchanged across all cohorts in the non-**stroma** compartment, signifying a stromal-specific response to PKC- β inhibition *in vivo*.

These data demonstrate that PKC- β mediated activation of TFEB and lysosome biogenesis in stromal cells are central for EMDR and the reciprocal stabilization of BCL-X_L in tumor cells.

Plasma membrane protein composition of stromal cells is regulated by PKC- β

Our gene expression profiling of stroma cells indicates a disparate cell surface phenotype between PKC- β WT and KO cells. To define the contribution of cell-cell interactions and response to venetoclax, we separated CLL cells from stromal cells using transwells. Disruption of cell-cell contact increased spontaneous apoptosis and venetoclax-induced cell death, indicating that cell-cell contact is of predominant importance for EMDR (Fig. 5A). To identify proteins on the surface of stromal cells relevant for contact-dependent survival of CLL cells, we performed plasma-membrane profiling (PMP) of MSCs, cultured in the absence or presence of CLL cells \pm enzastaurin. Quantitative proteomic analysis identified changes in the composition of cell surface proteins of MSCs induced by contact with CLL cells (Fig. 5B and data file S2). Importantly, inhibition of PKC- β with enzastaurin altered the expression of cell surface proteins of CLL-activated MSCs, whereby the amounts of 79 and 123 proteins were up- and down-regulated by enzastaurin (q -value <0.05), respectively. A cluster of proteins with increased CLL-dependent cell surface expression was appreciably reduced by enzastaurin (cluster 2), whereas the surface expression of other proteins was increased after treatment with the PKC- β inhibitor (clusters 1,3). Enzastaurin altered the expression of proteins that have potential roles in adhesion, including collagen1A2 and several matrix glycoproteins (Fig. 5C). In addition, surface proteins with a potential role for activating MSCs themselves were detected. The PKC- β dependent expression of IL1RI1, ADAM17 and IL6ST may contribute to the observed inflammatory gene signature of tumor-

cell activated MSCs(10). Importantly, PMP of MSCs indicated that VCAM1 was also down-regulated by enzastaurin. Flow cytometry analysis on primary MSCs from WT and KO mice demonstrated a significantly higher expression of VCAM1 on WT cells (Fig. 5D), which was down-regulated on CLL-activated stroma cells upon PKC- β kinase inhibition (fig. S7E). VCAM1 can bind to integrins expressed on a variety of leukocytes, contributing to cell adhesion and survival (28). We therefore hypothesized that diminished EMDR observed in KO stromal cells was partly attributed to a reduced expression of VCAM1. To test this, we generated Vcam1-deficient bone marrow MSCs using CRISPR/Cas9. Assessment of viability of CLL cells, co-cultured on Vcam1 proficient or deficient stromal cells, indicated that VCAM1 contributes to the anti-apoptotic effects on malignant B cells. This dependency was further augmented by treatment with venetoclax (Fig. 5E). Similarly, a blocking antibody against VCAM1 enhanced spontaneous and venetoclax-induced apoptosis of CLL cells, indicating that VCAM1 is important for EMDR (Fig. 5F). Importantly, overexpression of constitutively active TFEB not only rescued EMDR (Fig. 4I), but also partially restored VCAM1 expression on KO cells (Fig. 5G). **In support of this finding, deletion of TFEB caused a marked down-regulation of VCAM on stroma cells (Fig. 5H and fig. S7F)**, indicating that PKC- β -dependent activation of TFEB and lysosome biogenesis is important for plasma membrane integrity.

As a number of adhesion molecules were impacted by enzastaurin, we investigated whether blocking PKC- β resulted in a diminished capacity for adhesion of CLL cells *in vitro*. Patient CLL cells were flowed over PKC- β WT and KO stroma in defined channel slides (fig. S8A). Results indicated no difference existed between the adhesive capacity of both stromal genotypes in this assay (Fig. 5I, blue), with both stroma able to retain flowing CLL cells comparably equally and concordant with the *in vivo* homing data previously observed. Subsequently, treatment of adhered CLL on WT stroma with either vehicle or enzastaurin, demonstrated no difference in CLL cells mobilized in comparison between enzastaurin treated and untreated conditions. Additionally, KO stroma also showed comparable number of mobilized CLL cells upon channel flushing (Fig. 5I, red), indicating reduced Vcam1 expression does not impair stroma adhesion or retention of CLL under these conditions. To further validate this result, we treated diseased TCL1-tg mice for 2 consecutive days with enzastaurin before monitoring disease burden in the peripheral blood and lymphoid organs (Fig. 5J). In line with our *in vitro* data, we did not observe a mobilization of tumor cells into the peripheral blood. Likewise, disease burden in the peripheral blood, bone marrow, spleen and peritoneal cavity did not change over the course of the experiment (Fig. 5, K and L; fig. S8B and C). Notably, *in vivo* VCAM1 was markedly down-regulated on bone marrow derived CD45⁺Ter119⁻ **stroma cells** from enzastaurin treated mice to similar amounts found on cells

derived from KO mice (Fig. 5, M to O), indicating that the applied dose of enzastaurin was sufficient to inhibit stromal PKC- β *in vivo*. VCAM1 expression on bone marrow MSCs may therefore be a suitable and easily accessible biomarker for drug-efficacy in future studies.

In conclusion, our data show that PKC- β kinase activity regulates the expression of numerous adhesion molecules on stromal cells. Their pharmacological down-regulation by kinase inhibitors does not affect positioning of malignant B cells within lymphoid niches but reduces EMDR.

Enzastaurin enhances chemo-sensitivity and prolongs survival *in vivo*

Encouraged by these results, we tested whether the chemo-sensitizing effects of PKC- β inhibitors observed *in vitro* could be translated into the treatment of murine B cell malignancies. To this end, we transplanted 3.5 to 5×10^6 splenocytes from several individual, diseased *TCL1-tg* mice i.p. into 4 cohorts of syngeneic C57B/6 mice. Three days after transplantation, mice were orally treated for 16 consecutive days with either enzastaurin, venetoclax or a combination of both (treatment scheme is shown in fig. S9A). Treatment was well tolerated without hematotoxicity (fig. S9B) or weight loss. However, venetoclax treated mice developed a loss of hair pigmentation, which was markedly enhanced with enzastaurin co-administration (fig. S9C). This is a known on-target side effect of venetoclax, explained by the exquisite dependency of melanoblasts on BCL-2(29). Monitoring of leukemogenesis in the peripheral blood revealed single agent treatment with enzastaurin or venetoclax, given over the course of 16 days, had no effect on the number of tumor cells in the peripheral blood or disease progression. In stark contrast, combination treatment reduced tumor burden and terminal spleen weights, whilst prolonging the life expectancy of mice (Fig. 6, A and B; fig. S9D). **A separate assessment of BCL-X_L *in vivo* in tumor cells of diseased animals showed that venetoclax induced its expression as anticipated from *in vitro* experiments (Fig. 6C).**

Similar to venetoclax, mice were also treated with fludarabine in combination with enzastaurin (fig. S9E). Disease progression, monitored in the peripheral blood 25-28 days after initial treatment, showed tumor cells in both cohorts with difference between treatment groups ($32.4 \pm 3.4\%$ of circulating tumor cells in the fludarabine group vs. $9.6\% \pm 6.7\%$ in the combination treatment group (fig. S9F)). Mice were then treated with a second cycle of therapy, 54 days after transplantation. The concurrent treatment of fludarabine and enzastaurin markedly prolonged survival of mice compared to fludarabine mono-therapy (Fig. 6D). No increased hematotoxicity was observed in mice concurrently treated with enzastaurin (fig. S9, G and H).

Our *in vitro* data demonstrated that the chemo-sensitizing effects of enzastaurin were ablated in co-cultures of tumor- and PKC- β KO stroma cells, indicating that no off-target effects contributed to the enhanced cytotoxicity of venetoclax (Fig. 2F). To prove that no off-target effects by co-administered enzastaurin contribute to the survival benefits observed *in vivo*, we generated TCL-1 driven B cell lymphoma which could overcome the strong dependency of *E μ -TCL1-tg* cells on microenvironment PKC- β (Fig. 1). *E μ -TCL1-tg* mice were crossed onto transposon harboring mice expressing dual transposases PiggyBac and Sleeping Beauty (Hyper-GRONC, HG)(30, 31). Transplanted *TCL1-HG* tumors overcame loss of microenvironment PKC- β , though displayed delayed leukemic progression compared to PKC- β wild-type recipients receiving the same *TCL1-HG* cells (fig. S9I). After engraftment of B cell tumors from this mouse model in PKC- β KO animals, mice were subsequently treated with venetoclax or a combination of enzastaurin and venetoclax. Venetoclax treatment prolonged life expectancy of diseased KO recipient mice. Importantly, the addition of enzastaurin did not result in extended survival (Fig. 6E), indicating that the chemo-sensitizing effects of the PKC- β inhibitor were not attributed to off-target effects or on-target inhibition of tumor-PKC- β .

Based on our previous observation that PKC- β was also activated in stromal cells following contact to tumor cells from ALL and MCL patients(10), we investigated whether PKC- β inhibition in WT stromal cells mitigated EMDR of co-cultured primary B cells from ALL and MCL patients. Analogous to CLL, enzastaurin enhanced the therapeutic effect of venetoclax on MCL cells (Fig. 6F and table S1). To demonstrate a chemo-sensitizing effect of PKC- β inhibition on primary cells from ALL patients, enzastaurin was used in combination with dexamethasone or vincristine, both established chemotherapies in the treatment of ALL patients. Inhibition of stromal PKC- β with enzastaurin increased the cytotoxicity of both drugs (Fig. 6G and table S1). Importantly, this effect was completely abolished in co-cultures with KO stromal cells (Fig. 6H), confirming that the PKC- β inhibitor sensitized B-ALL cells by targeting stromal PKC- β and excludes the contribution of off-target effects or inhibitory effects on PKC- β expressed in ALL cells. To assess whether PKC- β inhibition also sensitizes primary ALL cells to chemotherapy *in vivo*, NSG mice xenografted with luciferase-labelled ALL-PDX cells were treated for 3 days with vincristine \pm enzastaurin. Bioluminescent imaging between 3 to 6 weeks post-transplantation revealed comparable leukemic burdens between vehicle and enzastaurin-treated mice (Fig. 6I and fig. S9J). As expected from our *in vitro* data, enzastaurin mono-therapy did not extend survival of ALL xenografted mice compared to vehicle controls, while the concomitant administration of enzastaurin and vincristine increased life-expectancy compared to single agent vincristine treatment (Fig. 6J).

In conclusion, enzastaurin increases the efficacy of different chemotherapy regimes *in vivo* by mitigating EMDR, demonstrated in pre-clinical CLL and ALL mouse models. In addition, ablation of EMDR by PKC- β inhibition was also observed in another B cells malignancy *in vitro*, indicating that the inhibition of PKC- β -dependent EMDR sensitizes a broad range of B cell malignancies to cytotoxic therapies.

DISCUSSION

A growing amount of research has identified tumor-host interactions as essential processes regulating tumor cell immune evasion, metabolic adaptations, survival and proliferation (32). Here we describe a crucial dependency for survival of normal B1- and malignant B cells on PKC- β expressed in stromal cells. Under conditions of cytotoxic stress PKC- β regulates lysosome-biogenesis by stabilizing TFEB, which is essential for plasma membrane composition and EMDR, effectuated by BCL-X_L expression in tumor cells. Genetic and pharmacological interference with this stress-response blunts this adaptation and increases the efficacy of chemotherapies (Fig. 7).

Since neither homing nor proliferation of malignant B cells was affected by the removal of PKC- β from the microenvironment, we hypothesize that the predominant role of stromal PKC- β is the provision of survival signals to these cells that are intermittently required throughout their life-time. Under conditions of cytotoxic stress, PKC- β -dependent MAPK-mediated up-regulation of BCL-X_L is essential for drug resistance and cell survival. However, it remains to be experimentally addressed whether similar mechanisms are in place under steady-state conditions and if so, to define their temporal and spatial requirements. It appears that the bone marrow is of particular importance for malignant B cells as the absence of PKC- β leads to a rapid loss of adoptively transferred cells in this compartment. This is in consonance with the clinical importance of this compartment for many B cells diseases, as reflected by the negative impact of bone marrow minimal-residual-disease (MRD)-positivity on progression-free-survival (7, 33). However, this conclusion is partly based on a lack of data, since MRD assessment in patients is restricted to easily accessible locations. Therefore, it remains unknown whether chemo-protective niches exist in other organs. While we have observed the strongest dependency on PKC- β in the bone marrow compartment during early disease stages, it is reasonable to assume that the spatial requirements and cellular composition of drug-protective niches are dynamic and change over time. In support of this hypothesis, in the E μ -TCL-1 model the spleen appears to be the predominant site of disease at a terminal stage. The marked reduction of the spleen size in enzastaurin co-treated mice suggests that drug-protective niches also exist in this organ and are possibly more relevant at later disease stages. Indeed, we found that splenic follicular

reticular cells (FRCs) can mediate PKC- β dependent drug resistance *in vitro*, similar to MSCs (fig S10A). Therefore, cell types other than bone marrow MSCs, present in different organs, are likely to also contribute to the observed effects *in vivo*. Their identification and molecular characterization is important and can be achieved through the employment of reporter mice.

In addition to tumor cells, we have observed that the physiological development of B1 cells also depends on PKC- β activity in the microenvironment. Although predominantly derived from fetal liver progenitors, B1 cells can also be derived from bone marrow HSCs(34, 35). Results from our bone marrow chimeras, showing impaired B1 cell development of WT bone marrow cells in a PKC- β KO background were unexpected and, in light of previously published data, indicate that PKC- β has a dual function in B cell development, maintenance and differentiation. Based on the observations made in germ-line deleted PKC- β KO mice(12), several groups have unambiguously demonstrated that *intrinsically* expressed PKC- β in B cells is essential for BCR-signaling through the recruitment of IKKs into lipid rafts and activation of IKK α / NF- κ B(36, 37). More recently, it was demonstrated that PKC- β deficient B cells fail to present antigens and to differentiate into plasma cells upon immunization (38). However, the capacity to form germinal centers *ex vivo* was *per se* not ablated in PKC- β KO B cells, indicating that the essential role of PKC- β for B cell differentiation is dependent on cell-cell interactions. A dual function of PKC- β in B cell physiology is also supported by our observation that WT bone marrow cells outperformed PKC- β KO cells in KO recipient mice with respect to the development of peritoneal B1 cells. In surprising contrast, the capacity of KO cells to produce B1 cells was indistinguishable from WT cells in WT recipient animals. In line with this observation, we found similar titers of the natural antibodies IgM and IgG3 in WT recipient animals reconstituted with KO CD45⁺ bone marrow cells. Although we cannot fully exclude the possibility that plasma cells survived lethal irradiation of recipient mice(39) and contribute to these antibody concentrations, reduced IgM and IgG3 titers in KO recipient animals reconstituted with WT CD45⁺ bone marrow cells strongly suggest that extrinsically expressed PKC- β is crucial for the production of natural antibodies. These findings reveal that the exquisite dependence of malignant B cells, especially under therapy, on PKC- β -dependent functions in their environment is already an integral part of normal B cell physiology.

Central to the environment-mediated drug resistance observed in our studies was a PKC- β -mediated increase in BCL-X_L expression, in response to various chemotherapeutics with differing mechanisms of drug action. It was previously recognized that BCL-X_L can confer a

multi-drug resistant phenotype in hematopoietic- (40) and non-hematopoietic cells (41), making it a key target for therapy. Interestingly, CLL cells respond to the cellular stress of BCL-2 antagonism by a microenvironment-mediated post-transcriptional increase in BCL-X_L expression. However, our data show that the increased BCL-X_L protein expression in CLL co-cultured with PKC-β WT stroma was not attributed to enhanced transcription. This raises questions about the underlying mechanisms causing an extrinsically-mediated increase of BCL-X_L protein. Different post-translational modifications of BCL-X_L, such as ubiquitination(42) and deamidation(43), must also be considered as possible contributing factors.

BCL-X_L was reported to be critical for the escape of self-reactive B-cells from negative selection: Self-reactive B-cells with enforced BCL-X_L expression were shown to have some hallmarks of receptor editing and were uniformly anergic, after central deletion escape (44). The correlative ERK1/2 activation we experimentally observed in CLL cells may also be indicative of an anergic program, which has been reported to favor survival(45, 46). We may speculate though that the cellular stress of BCL-2 inhibition could re-invoke a microenvironment-mediated anergic survival program previously utilized by self-reactive B-cells to escape central deletion. In line with this speculation Eμ-TCL1 cells that failed to engraft in PKC-β-deficient mice might have failed to increase BCL-X_L expression *in vivo* and succumbed to a retained autoimmunity checkpoint invoked by the absence of extrinsic PKC-β. Notwithstanding the exact physiological counterpart, we clearly demonstrate MEK1/2- or PKC-β inhibition represent very clinically attractive approaches to mitigate EMDR by preventing the up-regulation of BCL-X_L in the malignant cells.

Our experiments demonstrate that VCAM1 expression on stromal cells is exquisitely dependent on PKC-β-mediated activation of TFEB. **Previous studies have reported that the acute deletion of Vcam1 in adult mice led to a reduction of immature and mature B cells in the bone marrow (47, 48). In addition, homing of adoptively transferred mature B cells to the bone marrow was significantly impaired in these mice(47). In contrast, germ-line deletion of Vcam1, though is very often embryonic lethal, gave rise to a hypomorphic mouse model with no defects in B cell maturation (49), suggesting that low expression of VCAM1 is sufficient for B cell development or that compensatory mechanisms exist.** It is reasonable to assume that the reduced expression of VCAM1 on bone marrow MSCs of PKC-β-deficient mice contributes to the PKC-β-deficient phenotypes. The low expression of constitutive VCAM1 on mesenchymal cells of PKC-β KO mice is possibly related to reduced activity of NF-κB, as Vcam1 is a direct transcriptional target(50). We have previously demonstrated the PKC-β dependent activation of NF-κB in stromal cells, essential for tumor cell survival, is dependent

on Essential Modulator (NEMO)(10). Here we describe that the PKC- β dependent activation of TFEB and resultant lysosome biogenesis is of critical importance for plasma membrane composition and EMDR. Therefore, it is reasonable to speculate that the NF- κ B deficiency observed in PKC- β KO stromal cells is, at least partially, attributed to a lack of lysosome-mediated degradation of I κ B, as previously described(51, 52). However, lysosomes are multi-functional organelles, contributing to many cellular processes, including autophagy, exosome release, plasma membrane repair and adhesion. Therefore, other mechanisms may operate in parallel, including ECM-remodeling and enhanced integrin-signaling(53, 54), which could both further contribute to EMDR.

We believe that we have generated sufficient data to justify investigating the chemo-sensitizing properties of PKC- β inhibitors in a clinical setting. We have observed substantial survival benefits by co-administered enzastaurin in all our *in vivo* treatment experiments: Of note, our treatment with venetoclax was limited to 16 days. It can be expected that a continuous treatment with PKC- β inhibitors and venetoclax, as it is clinical practice in patients, will provide much greater survival benefits and deeper remissions. Similarly, the extended survival observed with combination treatment in our ALL-PDX model is a proof-of-principle that PKC- β inhibitors enhance the cytotoxic effects of vincristine. In contrast to the treatment of ALL patients, which receive cytotoxic therapies for 1-2 years, diseased animals received only a very short course of vincristine, which already lead to a substantial survival benefit. Enhanced effects of PKC- β inhibitors are therefore likely to be observed in clinical practice with repeated treatment cycles given to patients.

Conceptually similar to our proposed drug combinations, the concomitant treatment with BCL-2- and BTK-inhibitors is currently being investigated in lymphoma patients(55), aiming at blocking microenvironment interactions to enhance the cytotoxicity of venetoclax. Contrary to this concept, our data indicate that PKC- β inhibitors cause an “*in-situ chemo-sensitization*” of B cells as we have not observed an adherence-deficiency or a redistribution of cells into the peripheral blood upon kinase inhibition. The reduced expression of adhesion molecules on PKC- β deficient stromal cells likely reduces survival signals to leukemic cells, but without affecting niche residency. The dependency of different types of B cells, including normal B1 cells and immature malignant B cells, on PKC- β functions in the microenvironment, further indicates that PKC- β inhibitors may be clinically used beyond the spectrum of BCR-inhibitor sensitive disease entities. The treatment of auto-immune diseases with a pathogenic contribution from B cells, such as systemic lupus erythematosus, may also benefit from the chemo-sensitizing effects of PKC- β inhibitors.

At present, the PKC- β inhibitor enzastaurin, an oral ATP-competitive small molecule inhibitor with a relative specificity for PKC- β (16), is in clinical development at the stage of phase III

trials (e.g. NCT03263026). In addition, midostaurin, though less specific for the β -isoform, has recently been approved for the treatment of AML patients (18). Based on the observation that PKC- β is intrinsically expressed in malignant B cells, favorable phase II data and an excellent safety profile, the PRELUDE phase III trial was designed to test the efficacy of enzastaurin as maintenance mono-therapy for DLBCL patients in at least partial remission following treatment with R-CHOP. The trial failed its primary end point (disease free survival)(56), which led to a temporary halt in the clinical development of the drug. Notably, contrary to low-grade lymphomas or ALL, MRD is clinically not a problem for the vast majority of DLBCL patients, suggesting that EMDR may not play a substantial role for the majority of patients with high-grade NHL. This is reflected by the observation that 70% of patients in the PRELUDE trial were already cured at the end of immuno-chemotherapy, before commencing maintenance therapy.

Our data provide evidence that the chemo-sensitizing effects of enzastaurin depend on the lysosome-mediated remodeling of cell-surface and matrix-proteins. Since enzastaurin undergoes liver-mediated degradation and has a short half-life(57), contributing to a substantial inter-subject variability in the steady-state plasma concentration(58), we predict that the timing between administering a PKC- β inhibitor to mitigate EMDR and cytotoxic agents are important for their synergism. Biomarkers such as VCAM1 or LAMP1 expression in MSCs should therefore be used in future clinical trials to determine the optimal time between co-administering chemo-sensitizing- and cytotoxic therapy.

The incorporation of PKC- β inhibitors in treatment-regimens used for various B cells malignancies may have profound clinical and socioeconomic implications: improved clinical responses may ultimately allow for the reduction of the number of treatment cycles, lowering cumulative drug doses and minimizing side effects, costs and need for salvage therapies. Notably our data demonstrate that the application of PKC- β inhibitors can be limited to treatment days, minimizing their compound-specific side effects and costs. Clinical trials are now needed to address whether our data can be translated into improved patient care.

MATERIAL AND METHODS

STUDY DESIGN

Our primary objective was to test whether the dependency of malignant B cells from patients with CLL, MCL and ALL patients on PKC- β expressed and activated in the tumor microenvironment could be harnessed therapeutically. By transferring normal bone marrow or labeled tumor cells into WT and KO recipient mice we demonstrate that stroma PKC- β is required for normal B1 cell development and the survival of malignant B cells. This dependency was further investigated through *ex vivo* co-culture experiments, in which we demonstrate that small molecule inhibitors targeting PKC- β mitigate environment mediated drug resistance by blocking the up-regulation of BCL-X_L in tumor cells in an ERK and PI3K dependent manner. We employed RNAseq and mass spectrometry to delineate the molecular mechanisms in stromal cells, demonstrating that stromal PKC- β is essential for the activation of TFEB. Activated TFEB in stromal cells regulates the expression of adhesion molecules required for stroma-mediated protection from cytotoxic agents. Our data were validated through *in vivo* experiments, in which diseased C57B/6 or NSG- mice were treated with cytotoxic agents in combination with PKC- β inhibitors.

We did not use statistics to predetermine sample sizes. Animals were randomly assigned to genotypes or the 4 treatment cohorts (vehicle control, venetoclax or vincristine, enzastaurin, enzastaurin + venetoclax or vincristine). Sample sizes in the mouse experiments were based on own and published data (10, 59). Animal wellbeing was monitored daily and all experiments were conducted under the UK Home Office regulations. Investigators were not blinded to treatment allocations, but animal technicians who delivered care and decided independently upon which animals needed to be sacrificed (applying strict criteria for end points) were blinded. *In vitro* studies were conducted with multiple technical and biological replicates to ensure reproducibility of data.

STATISTICAL ANALYSES

All *in vitro* experiments were repeated at least three times, and the means \pm SEM were calculated. The exact sample size for each experiment is provided in the figure legends. Statistical analyses of results were performed using one-way ANOVA followed by two-tail Student t-tests, with respective unpaired and paired analyses experimentally dependent. Statistical annotations as previously noted were denoted with asterisks according to the following, ****p < 0.0001, *** p <0.001, **p<0.01, *p<0.05, and ns p >0.05. *In vivo* studies were carried out using multiple animals (3 to 15 per group, specified in figures), and Kaplan-Meier curves were generated from survival data.

SUPPLEMENTARY MATERIALS

Material and Methods

Figure S1: Homing and engraftment kinetics of E μ -TCL1 CLL in PKC- β wild-type and null mice.

Figure S2: PKC- β deficiency does not overtly alter hematopoiesis.

Figure S3: PKC- β chimeras engraft with comparable efficiency irrespective of donor or recipient genotype.

Figure S4: Monocytes confer CLL survival support but not PKC- β dependent EMDR, in contrast to MSCs.

Figure S5: PKC- β -mediated EMDR involves increased protein levels of BCL-X_L.

Figure S6: CLL signaling pathways regulated by stromal PKC- β correlate with clinical outcomes.

Figure S7: Stromal lysosomes, and lysosomal biogenesis regulator TFEB, are central to PKC- β -mediated EMDR.

Figure S8: PKC- β is dispensable for *in vitro* and *in vivo* mobilization of leukemia.

Figure S9: *In vivo* co-targeting of PKC- β does not contribute to increased off-target cytotoxicity.

Figure S10: EMDR derived from splenic stroma is mitigated by PKC- β antagonism.

Figure S11: Representative FACS gating strategies.

Table S1: Patient characteristics.

Table S2: Key resources.

Data File S1: Excel file of top deregulated genes from CLL RNA-Seq in Fig.3C

Data File S2: Excel file of proteomic clusters from Fig. 5B,C.

Data File S3: Excel file of individual data from experiments with n<20 per group.

References (60-68)

REFERENCES AND NOTES

1. X. S. Puente, M. Pinyol, V. Quesada, L. Conde, G. R. Ordóñez, N. Villamor, G. Escaramis, P. Jares, S. Beà, M. González-Díaz, L. Bassaganyas, T. Baumann, M. Juan, M. López-Guerra, D. Colomer, J. M. C. Tubío, C. López, A. Navarro, C. Tornador, M. Aymerich, M. Rozman, J. M. Hernández, D. A. Puente, J. M. P. Freije, G. Velasco, A. Gutiérrez-Fernández, D. Costa, A. Carrió, S. Guijarro, A. Enjuanes, L. Hernández, J. Yagüe, P. Nicolás, C. M. Romeo-Casabona, H. Himmelbauer, E. Castillo, J. C. Dohm, S. de Sanjosé, M. A. Piris, E. de Alava, J. San Miguel, R. Royo, J. L. Gelpí, D. Torrents, M. Orozco, D. G. Pisano, A. Valencia, R. Guigó, M. Bayés, S. Heath, M. Gut, P. Klatt, J. Marshall, K. Raine, L. A. Stebbings, P. A. Futreal, M. R. Stratton, P. J. Campbell, I. Gut, A. López-Guillermo, X. Estivill, E. Montserrat, C. López-Otín, E. Campo, Whole-genome sequencing identifies recurrent mutations in chronic lymphocytic leukaemia, *Nature* **475**, 101–105 (2011).
2. V. Quesada, L. Conde, N. Villamor, G. R. Ordóñez, P. Jares, L. Bassaganyas, A. J. Ramsay, S. Beà, M. Pinyol, A. Martínez-Trillos, M. López-Guerra, D. Colomer, A. Navarro, T. Baumann, M. Aymerich, M. Rozman, J. Delgado, E. Giné, J. M. Hernández, M. González-Díaz, D. A. Puente, G. Velasco, J. M. P. Freije, J. M. C. Tubío, R. Royo, J. L. Gelpí, M. Orozco, D. G. Pisano, J. Zamora, M. Vázquez, A. Valencia, H. Himmelbauer, M. Bayés, S. Heath, M. Gut, I. Gut, X. Estivill, A. López-Guillermo, X. S. Puente, E. Campo, C. López-Otín, Exome sequencing identifies recurrent mutations of the splicing factor SF3B1 gene in chronic lymphocytic leukemia, *Nat. Genet.* **44**, 47–52 (2012).
3. B. Chapuy, C. Stewart, A. J. Dunford, J. Kim, A. Kamburov, R. A. Redd, M. S. Lawrence, M. G. M. Roemer, A. J. Li, M. Ziepert, A. M. Staiger, J. A. Wala, M. D. Ducar, I. Leshchiner, E. Rheinbay, A. Taylor-Weiner, C. A. Coughlin, J. M. Hess, C. S. Pedomallu, D. Livitz, D. Rosebrock, M. Rosenberg, A. A. Tracy, H. Horn, P. van Hummelen, A. L. Feldman, B. K. Link, A. J. Novak, J. R. Cerhan, T. M. Habermann, R. Siebert, A. Rosenwald, A. R. Thorner, M. L. Meyerson, T. R. Golub, R. Beroukhim, G. G. Wulf, G. Ott, S. J. Rodig, S. Monti, D. S. Neuberg, M. Loeffler, M. Pfreundschuh, L. Trümper, G. Getz, M. A. Shipp, Molecular subtypes of diffuse large B cell lymphoma are associated with distinct pathogenic mechanisms and outcomes, *Nat. Med.* **24**, 679–690 (2018).
4. R. Schmitz, G. W. Wright, D. W. Huang, C. A. Johnson, J. D. Phelan, J. Q. Wang, S. Roulland, M. Kasbekar, R. M. Young, A. L. Shaffer, D. J. Hodson, W. Xiao, X. Yu, Y. Yang, H. Zhao, W. Xu, X. Liu, B. Zhou, W. Du, W. C. Chan, E. S. Jaffe, R. D. Gascoyne, J. M. Connors, E. Campo, A. López-Guillermo, A. Rosenwald, G. Ott, J. Delabie, L. M. Rimsza, K. Tay Kuang Wei, A. D. Zelenetz, J. P. Leonard, N. L. Bartlett, B. Tran, J. Shetty, Y. Zhao, D. R. Soppet, S. Pittaluga, W. H. Wilson, L. M. Staudt, Genetics and Pathogenesis of Diffuse Large B-Cell Lymphoma, *N. Engl. J. Med.* **378**, 1396–1407 (2018).
5. M. B. Meads, R. A. Gatenby, W. S. Dalton, Environment-mediated drug resistance: a major contributor to minimal residual disease, *Nat. Rev. Cancer* **9**, 665–674 (2009).
6. D. A. Berry, S. Zhou, H. Higley, L. Mukundan, S. Fu, G. H. Reaman, B. L. Wood, G. J. Kelloff, J. M. Jessup, J. P. Radich, Association of Minimal Residual Disease With Clinical Outcome in Pediatric and Adult Acute Lymphoblastic Leukemia: A Meta-analysis, *JAMA Oncol* **3**, e170580–e170580 (2017).
7. S. Böttcher, M. Ritgen, K. Fischer, S. Stilgenbauer, R. M. Busch, G. Fingerle-Rowson, A. M. Fink, A. Bühler, T. Zenz, M. K. Wenger, M. Mendila, C.-M. Wendtner, B. F. Eichhorst, H. Döhner, M. J. Hallek, M. Kneba, Minimal residual disease quantification is an independent predictor of progression-free and overall survival in chronic lymphocytic leukemia: a multivariate analysis from the randomized GCLLSG CLL8 trial, *J. Clin. Oncol.* **30**, 980–988

(2012).

8. B. Löwenberg, W. van Putten, M. Theobald, J. Gmür, L. Verdonck, P. Sonneveld, M. Fey, H. Schouten, G. de Greef, A. Ferrant, T. Kovacsovics, A. Gratwohl, S. Daenen, P. Huijgens, M. Boogaerts, Dutch-Belgian Hemato-Oncology Cooperative Group, Swiss Group for Clinical Cancer Research, Effect of priming with granulocyte colony-stimulating factor on the outcome of chemotherapy for acute myeloid leukemia, *N. Engl. J. Med.* **349**, 743–752 (2003).

9. G. J. Ossenkoppele, G. Stussi, J. Maertens, K. van Montfort, B. J. Biemond, D. Breems, A. Ferrant, C. Graux, G. E. de Greef, C. J. M. Halkes, M. Hoogendoorn, R. M. Hollestein, M. Jongen-Lavrencic, M. D. Levin, A. A. van de Loosdrecht, M. van Marwijk Kooij, Y. van Norden, T. Pabst, H. C. Schouten, E. Vellenga, G. E. G. Verhoef, O. de Weerd, P. Wijermans, J. R. Passweg, B. Löwenberg, Addition of bevacizumab to chemotherapy in acute myeloid leukemia at older age: a randomized phase 2 trial of the Dutch-Belgian Cooperative Trial Group for Hemato-Oncology (HOVON) and the Swiss Group for Clinical Cancer Research (SAKK), *Blood* **120**, 4706–4711 (2012).

10. G. Lutzny, T. Kocher, M. Schmidt-Suppran, M. Rudelius, L. Klein-Hitpass, A. J. Finch, J. Dürig, M. Wagner, C. Haferlach, A. Kohlmann, S. Schnittger, M. Seifert, S. Wanninger, N. Zaborsky, R. Oostendorp, J. Ruland, M. Leitges, T. Kuhnt, Y. Schäfer, B. Lampl, C. Peschel, A. Egle, I. Ringshausen, Protein kinase c- β -dependent activation of NF- κ B in stromal cells is indispensable for the survival of chronic lymphocytic leukemia B cells in vivo, *Cancer Cell* **23**, 77–92 (2013).

11. R. Bichi, S. A. Shinton, E. S. Martin, A. Koval, G. A. Calin, R. Cesari, G. Russo, R. R. Hardy, C. M. Croce, Human chronic lymphocytic leukemia modeled in mouse by targeted TCL1 expression, *Proc. Natl. Acad. Sci. U.S.A.* **99**, 6955–6960 (2002).

12. M. Leitges, C. Schmedt, R. Guinamard, J. Davoust, S. Schaal, S. Stabel, A. Tarakhovsky, Immunodeficiency in protein kinase c β -deficient mice, *Science* **273**, 788–791 (1996).

13. R. R. Hardy, K. Hayakawa, B cell development pathways, *Annu. Rev. Immunol.* **19**, 595–621 (2001).

14. M. Seifert, L. Sellmann, J. Bloehdorn, F. Wein, S. Stilgenbauer, J. Dürig, R. Küppers, Cellular origin and pathophysiology of chronic lymphocytic leukemia, *J. Exp. Med.* **209**, 2183–2198 (2012).

15. M. Seiffert, A. Schulz, S. Ohl, H. Döhner, S. Stilgenbauer, P. Lichter, Soluble CD14 is a novel monocyte-derived survival factor for chronic lymphocytic leukemia cells, which is induced by CLL cells in vitro and present at abnormally high levels in vivo, *Blood* **116**, 4223–4230 (2010).

16. M. M. Faul, J. R. Gillig, M. R. Jirousek, L. M. Ballas, T. Schotten, A. Kahl, M. Mohr, Acyclic N-(azacycloalkyl)bisindolylmaleimides: isozyme selective inhibitors of PKC β , *Bioorg. Med. Chem. Lett.* **13**, 1857–1859 (2003).

17. J. Wagner, P. von Matt, R. Sedrani, R. Albert, N. Cooke, C. Ehrhardt, M. Geiser, G. Rummel, W. Stark, A. Strauss, S. W. Cowan-Jacob, C. Beerli, G. Weckbecker, J.-P. Evenou, G. Zenke, S. Cottens, Discovery of 3-(1H-indol-3-yl)-4-[2-(4-methylpiperazin-1-yl)quinazolin-4-yl]pyrrole-2,5-dione (AEB071), a potent and selective inhibitor of protein kinase C isotypes, *J. Med. Chem.* **52**, 6193–6196 (2009).

18. R. M. Stone, S. J. Mandrekar, B. L. Sanford, K. Laumann, S. Geyer, C. D. Bloomfield, C. Thiede, T. W. Prior, K. Döhner, G. Marcucci, F. Lo-Coco, R. B. Klisovic, A. Wei, J. Sierra, M. A. Sanz, J. M. Brandwein, T. de Witte, D. Niederwieser, F. R. Appelbaum, B. C. Medeiros, M. S. Tallman, J. Krauter, R. F. Schlenk, A. Ganser, H. Serve, G. Ehninger, S. Amadori, R. A. Larson, H. Döhner, Midostaurin plus Chemotherapy for Acute Myeloid Leukemia with a FLT3 Mutation, *N. Engl. J. Med.* **377**, 454–464 (2017).
19. G. Y. Di Veroli, C. Fornari, D. Wang, S. Mollard, J. L. Bramhall, F. M. Richards, D. I. Jodrell, Combenefit: an interactive platform for the analysis and visualization of drug combinations, *Bioinformatics* **32**, 2866–2868 (2016).
20. D. El-Gamal, K. Williams, T. D. LaFollette, M. Cannon, J. S. Blachly, Y. Zhong, J. A. Woyach, E. Williams, F. T. Awan, J. Jones, L. Andritsos, K. Maddocks, C.-H. Wu, C.-S. Chen, A. Lehman, X. Zhang, R. Lapalombella, J. C. Byrd, PKC- β as a therapeutic target in CLL: PKC inhibitor AEB071 demonstrates preclinical activity in CLL, *Blood* **124**, 1481–1491 (2014).
21. K. Bojarczuk, K. Wienand, J. A. Ryan, L. Chen, M. Villalobos-Ortiz, E. Mandato, J. Stachura, A. Letai, L. N. Lawton, B. Chapuy, M. A. Shipp, Targeted inhibition of PI3K α/δ is synergistic with BCL-2 blockade in genetically defined subtypes of DLBCL, *Blood* **133**, 70–80 (2019).
22. G. S. Choudhary, S. Al-Harbi, S. Mazumder, B. T. Hill, M. R. Smith, J. Bodo, E. D. Hsi, A. Almasan, MCL-1 and BCL-xL-dependent resistance to the BCL-2 inhibitor ABT-199 can be overcome by preventing PI3K/AKT/mTOR activation in lymphoid malignancies, *Cell Death Dis* **6**, e1593–e1593 (2015).
23. S. Stilgenbauer, T. Zenz, D. Winkler, A. Bühler, R. F. Schlenk, S. Groner, R. Busch, M. Hensel, U. Dührsen, J. Finke, P. Dreger, U. Jäger, E. Lengfelder, K. Hohloch, U. Söling, R. Schlag, M. Kneba, M. Hallek, H. Döhner, German Chronic Lymphocytic Leukemia Study Group, Subcutaneous alemtuzumab in fludarabine-refractory chronic lymphocytic leukemia: clinical results and prognostic marker analyses from the CLL2H study of the German Chronic Lymphocytic Leukemia Study Group, *J. Clin. Oncol.* **27**, 3994–4001 (2009).
24. M. Ferron, C. Settembre, J. Shimazu, J. Lacombe, S. Kato, D. J. Rawlings, A. Ballabio, G. Karsenty, A RANKL-PKC β -TFEB signaling cascade is necessary for lysosomal biogenesis in osteoclasts, *Genes Dev.* **27**, 955–969 (2013).
25. Y. Li, M. Xu, X. Ding, C. Yan, Z. Song, L. Chen, X. Huang, X. Wang, Y. Jian, G. Tang, C. Tang, Y. Di, S. Mu, X. Liu, K. Liu, T. Li, Y. Wang, L. Miao, W. Guo, X. Hao, C. Yang, Protein kinase C controls lysosome biogenesis independently of mTORC1, *Nat. Cell Biol.* **18**, 1065–1077 (2016).
26. Signals from the lysosome: a control centre for cellular clearance and energy metabolism, *Nat. Rev. Mol. Cell Biol.* **14**, 283–296 (2013).
27. N. P. Young, A. Kamireddy, J. L. Van Nostrand, L. J. Eichner, M. N. Shokhirev, Y. Dayn, R. J. Shaw, AMPK governs lineage specification through Tfeb-dependent regulation of lysosomes, *Genes Dev.* **30**, 535–552 (2016).
28. M. J. Elices, L. Osborn, Y. Takada, C. Crouse, S. Luhowskyj, M. E. Hemler, R. R. Lobb, VCAM-1 on activated endothelium interacts with the leukocyte integrin VLA-4 at a site distinct from the VLA-4/fibronectin binding site, *Cell* **60**, 577–584 (1990).
29. S. Kamada, A. Shimono, Y. Shinto, T. Tsujimura, T. Takahashi, T. Noda, Y. Kitamura, H.

- Kondoh, Y. Tsujimoto, bcl-2 deficiency in mice leads to pleiotropic abnormalities: accelerated lymphoid cell death in thymus and spleen, polycystic kidney, hair hypopigmentation, and distorted small intestine, *Cancer Res.* **55**, 354–359 (1995).
30. G. S. Vassiliou, J. L. Cooper, R. Rad, J. Li, S. Rice, A. Uren, L. Rad, P. Ellis, R. Andrews, R. Banerjee, C. Grove, W. Wang, P. Liu, P. Wright, M. Arends, A. Bradley, Mutant nucleophosmin and cooperating pathways drive leukemia initiation and progression in mice, *Nat. Genet.* **43**, 470–475 (2011).
31. M. J. Friedrich, L. Rad, I. F. Bronner, A. Strong, W. Wang, J. Weber, M. Mayho, H. Ponstingl, T. Engleitner, C. Grove, A. Pfau, D. Saur, J. Cadiñanos, M. A. Quail, G. S. Vassiliou, P. Liu, A. Bradley, R. Rad, Genome-wide transposon screening and quantitative insertion site sequencing for cancer gene discovery in mice, *Nat Protoc* **12**, 289–309 (2017).
32. D. Hanahan, L. M. Coussens, Accessories to the crime: functions of cells recruited to the tumor microenvironment, *Cancer Cell* **21**, 309–322 (2012).
33. N. Gökbüget, M. Kneba, T. Raff, H. Trautmann, C.-R. Bartram, R. Arnold, R. Fietkau, M. Freund, A. Ganser, W.-D. Ludwig, G. Maschmeyer, H. Rieder, S. Schwartz, H. Serve, E. Thiel, M. Brüggemann, D. Hoelzer, German Multicenter Study Group for Adult Acute Lymphoblastic Leukemia, Adult patients with acute lymphoblastic leukemia and molecular failure display a poor prognosis and are candidates for stem cell transplantation and targeted therapies, *Blood* **120**, 1868–1876 (2012).
34. B. L. Esplin, R. S. Welner, Q. Zhang, L. A. Borghesi, P. W. Kincade, A differentiation pathway for B1 cells in adult bone marrow, *Proc. Natl. Acad. Sci. U.S.A.* **106**, 5773–5778 (2009).
35. S. Düber, M. Hafner, M. Krey, S. Lienenklaus, B. Roy, E. Hobeika, M. Reth, T. Buch, A. Waisman, K. Kretschmer, S. Weiss, Induction of B-cell development in adult mice reveals the ability of bone marrow to produce B-1a cells, *Blood* **114**, 4960–4967 (2009).
36. T. T. Su, B. Guo, Y. Kawakami, K. Sommer, K. Chae, L. A. Humphries, R. M. Kato, S. Kang, L. Patrone, R. Wall, M. Teitell, M. Leitges, T. Kawakami, D. J. Rawlings, PKC-beta controls I kappa B kinase lipid raft recruitment and activation in response to BCR signaling, *Nat. Immunol.* **3**, 780–786 (2002).
37. K. Saijo, I. Mecklenbräuker, A. Santana, M. Leitger, C. Schmedt, A. Tarakhovsky, Protein kinase C beta controls nuclear factor kappaB activation in B cells through selective regulation of the I kappaB kinase alpha, *J. Exp. Med.* **195**, 1647–1652 (2002).
38. C. Tsui, N. Martinez-Martin, M. Gaya, P. Maldonado, M. Llorian, N. M. Legrave, M. Rossi, J. I. MacRae, A. J. Cameron, P. J. Parker, M. Leitges, A. Bruckbauer, F. D. Batista, Protein Kinase C- β Dictates B Cell Fate by Regulating Mitochondrial Remodeling, Metabolic Reprogramming, and Heme Biosynthesis, *Immunity* (2018), doi:10.1016/j.immuni.2018.04.031.
39. J. J. Miller, L. J. Cole, The radiation resistance of long-lived lymphocytes and plasma cells in mouse and rat lymph nodes, *J. Immunol.* **98**, 982–990 (1967).
40. A. J. Minn, C. M. Rudin, L. H. Boise, C. B. Thompson, Expression of bcl-xL can confer a multidrug resistance phenotype, *Blood* **86**, 1903–1910 (1995).
41. S. A. Amundson, T. G. Myers, D. Scudiero, S. Kitada, J. C. Reed, A. J. Fornace, An informatics approach identifying markers of chemosensitivity in human cancer cell lines,

Cancer Res. **60**, 6101–6110 (2000).

42. R. Kajihara, H. Sakamoto, K. Tanabe, K. Takemoto, M. Tasaki, Y. Ando, S. Inui, Protein phosphatase 6 controls BCR-induced apoptosis of WEHI-231 cells by regulating ubiquitination of Bcl-xL, *J. Immunol.* **192**, 5720–5729 (2014).

43. B. E. Deverman, B. L. Cook, S. R. Manson, R. A. Niederhoff, E. M. Langer, I. Rosová, L. A. Kulans, X. Fu, J. S. Weinberg, J. W. Heinecke, K. A. Roth, S. J. Weintraub, Bcl-xL deamidation is a critical switch in the regulation of the response to DNA damage, *Cell* **111**, 51–62 (2002).

44. W. Fang, B. C. Weintraub, B. Dunlap, P. Garside, K. A. Pape, M. K. Jenkins, C. C. Goodnow, D. L. Mueller, T. W. Behrens, Self-reactive B lymphocytes overexpressing Bcl-xL escape negative selection and are tolerized by clonal anergy and receptor editing, *Immunity* **9**, 35–45 (1998).

45. B. Apollonio, C. Scielzo, M. T. S. Bertilaccio, E. Ten Hacken, L. Scarfò, P. Raghetti, F. Stevenson, G. Packham, P. Ghia, M. Muzio, F. Caligaris-Cappio, Targeting B-cell anergy in chronic lymphocytic leukemia, *Blood* **121**, 3879–88– S1–8 (2013).

46. M. Muzio, B. Apollonio, C. Scielzo, M. Frenquelli, I. Vandoni, V. Boussiotis, F. Caligaris-Cappio, P. Ghia, Constitutive activation of distinct BCR-signaling pathways in a subset of CLL patients: a molecular signature of anergy, *Blood* **112**, 188–195 (2008).

47. C. E. Leuker, M. Labow, W. Müller, N. Wagner, Neonatally induced inactivation of the vascular cell adhesion molecule 1 gene impairs B cell localization and T cell-dependent humoral immune response, *J. Exp. Med.* **193**, 755–768 (2001).

48. P. A. Koni, S. K. Joshi, U. A. Temann, D. Olson, L. Burkly, R. A. Flavell, Conditional vascular cell adhesion molecule 1 deletion in mice: impaired lymphocyte migration to bone marrow, *J. Exp. Med.* **193**, 741–754 (2001).

49. C. Friedrich, M. I. Cybulsky, J. C. Gutierrez-Ramos, Vascular cell adhesion molecule-1 expression by hematopoiesis-supporting stromal cells is not essential for lymphoid or myeloid differentiation in vivo or in vitro, *Eur. J. Immunol.* **26**, 2773–2780 (1996).

50. H. B. Shu, A. B. Agranoff, E. G. Nabel, K. Leung, C. S. Duckett, A. S. Neish, T. Collins, G. J. Nabel, Differential regulation of vascular cell adhesion molecule 1 gene expression by specific NF-kappa B subunits in endothelial and epithelial cells, *Mol. Cell. Biol.* **13**, 6283–6289 (1993).

51. A. M. Cuervo, W. Hu, B. Lim, J. F. Dice, I kappa B is a substrate for a selective pathway of lysosomal proteolysis, *Mol. Biol. Cell* **9**, 1995–2010 (1998).

52. L.-Y. Chu, Y.-C. Hsueh, H.-L. Cheng, K. K. Wu, Cytokine-induced autophagy promotes long-term VCAM-1 but not ICAM-1 expression by degrading late-phase IκBα, *Sci Rep* **7**, 12472 (2017).

53. V. Gocheva, W. Zeng, D. Ke, D. Klimstra, T. Reinheckel, C. Peters, D. Hanahan, J. A. Joyce, Distinct roles for cysteine cathepsin genes in multistage tumorigenesis, *Genes Dev.* **20**, 543–556 (2006).

54. L. Akkari, V. Gocheva, J. C. Kester, K. E. Hunter, M. L. Quick, L. Sevenich, H.-W. Wang, C. Peters, L. H. Tang, D. S. Klimstra, T. Reinheckel, J. A. Joyce, Distinct functions of macrophage-derived and cancer cell-derived cathepsin Z combine to promote tumor

- malignancy via interactions with the extracellular matrix, *Genes Dev.* **28**, 2134–2150 (2014).
55. C. S. Tam, M. A. Anderson, C. Pott, R. Agarwal, S. Handunnetti, R. J. Hicks, K. Burbury, G. Turner, J. Di Iulio, M. Bressel, D. Westerman, S. Lade, M. Dreyling, S.-J. Dawson, M. A. Dawson, J. F. Seymour, A. W. Roberts, Ibrutinib plus Venetoclax for the Treatment of Mantle-Cell Lymphoma, *N. Engl. J. Med.* **378**, 1211–1223 (2018).
56. M. Crump, S. Leppa, L. Fayad, J. J. Lee, A. Di Rocco, M. Ogura, H. Hagberg, F. Schnell, R. Rifkin, A. Mackensen, F. Offner, L. Pinter-Brown, S. Smith, K. Tobinai, S.-P. Yeh, E. D. Hsi, T. Nguyen, P. Shi, M. Hahka-Kemppinen, D. Thornton, B. Lin, B. Kahl, N. Schmitz, K. J. Savage, T. Habermann, Randomized, Double-Blind, Phase III Trial of Enzastaurin Versus Placebo in Patients Achieving Remission After First-Line Therapy for High-Risk Diffuse Large B-Cell Lymphoma, *J. Clin. Oncol.* **34**, 2484–2492 (2016).
57. P. A. Welch, V. P. Sinha, A. L. Cleverly, C. Darstein, S. D. Flanagan, L. C. Musib, Safety, tolerability, QTc evaluation, and pharmacokinetics of single and multiple doses of enzastaurin HCl (LY317615), a protein kinase C-beta inhibitor, in healthy subjects, *J Clin Pharmacol* **47**, 1138–1151 (2007).
58. M. A. Carducci, L. Musib, M. S. Kies, R. Pili, M. Truong, J. R. Brahmer, P. Cole, R. Sullivan, J. Riddle, J. Schmidt, N. Enas, V. Sinha, D. E. Thornton, R. S. Herbst, Phase I dose escalation and pharmacokinetic study of enzastaurin, an oral protein kinase C beta inhibitor, in patients with advanced cancer, *J. Clin. Oncol.* **24**, 4092–4099 (2006).
59. N. L. M. Liem, R. A. Papa, C. G. Milross, M. A. Schmid, M. Tajbakhsh, S. Choi, C. D. Ramirez, A. M. Rice, M. Haber, M. D. Norris, K. L. MacKenzie, R. B. Lock, Characterization of childhood acute lymphoblastic leukemia xenograft models for the preclinical evaluation of new therapies, *Blood* **103**, 3905–3914 (2004).
60. L. Wang, S. Wang, W. Li, RSeQC: quality control of RNA-seq experiments, *Bioinformatics* **28**, 2184–2185 (2012).
61. A. Dobin, C. A. Davis, F. Schlesinger, J. Drenkow, C. Zaleski, S. Jha, P. Batut, M. Chaisson, T. R. Gingeras, STAR: ultrafast universal RNA-seq aligner, *Bioinformatics* **29**, 15–21 (2013).
62. S. Anders, P. T. Pyl, W. Huber, HTSeq--a Python framework to work with high-throughput sequencing data, *Bioinformatics* **31**, 166–169 (2015).
63. M. I. Love, W. Huber, S. Anders, Moderated estimation of fold change and dispersion for RNA-seq data with DESeq2, *Genome Biol.* **15**, 550 (2014).
64. A. Sturn, J. Quackenbush, Z. Trajanoski, Genesis: cluster analysis of microarray data, *Bioinformatics* **18**, 207–208 (2002).
65. M. P. Weekes, S. Y. L. Tan, E. Poole, S. Talbot, R. Antrobus, D. L. Smith, C. Montag, S. P. Gygi, J. H. Sinclair, P. J. Lehner, Latency-associated degradation of the MRP1 drug transporter during latent human cytomegalovirus infection, *Science* **340**, 199–202 (2013).
66. E. J. Greenwood, N. J. Matheson, K. Wals, D. J. van den Boomen, R. Antrobus, J. C. Williamson, P. J. Lehner, Temporal proteomic analysis of HIV infection reveals remodelling of the host phosphoproteome by lentiviral Vif variants, *Elife* **5**, 12112 (2016).
67. R. Pan, L. J. Hogdal, J. M. Benito, D. Bucci, L. Han, G. Borthakur, J. Cortes, D. J. DeAngelo, L. Debose, H. Mu, H. Döhner, V. I. Gaidzik, I. Galinsky, L. S. Golfman, T.

Haferlach, K. G. Harutyunyan, J. Hu, J. D. Levenson, G. Marcucci, M. Müschen, R. Newman, E. Park, P. P. Ruvolo, V. Ruvolo, J. Ryan, S. Schindela, P. Zweidler-McKay, R. M. Stone, H. Kantarjian, M. Andreeff, M. Konopleva, A. G. Letai, Selective BCL-2 inhibition by ABT-199 causes on-target cell death in acute myeloid leukemia, *Cancer Discov* **4**, 362–375 (2014).

68. N. L. M. Liem, R. A. Papa, C. G. Milross, M. A. Schmid, M. Tajbakhsh, S. Choi, C. D. Ramirez, A. M. Rice, M. Haber, M. D. Norris, K. L. MacKenzie, R. B. Lock, Characterization of childhood acute lymphoblastic leukemia xenograft models for the preclinical evaluation of new therapies, *Blood* **103**, 3905–3914 (2004).

ACKNOWLEDGEMENTS

We would like to express our deepest gratitude to patients who donated blood for research purposes. In particular, we thank Joanna Baxter and her team for enrolling patients in these studies. We would like to thank Anthony Green, Brian Huntly, George Vassiliou and Dan Hodson for scientific discussion. We are thankful for the generous provision of Nestin^{GFP} mice by Simon Mendez-Ferrer and the help of Claudia Korn for staining bone marrow sections. Eμ-TCL1-tg mice were kindly provided by Carlo Croce under an MTA.

FUNDING

This work was funded by Cancer Research UK (CRUK; C49940/A17480). I.R. is a senior CRUK fellow. M.S.S is supported by the DFG through SCHM2440/7-1 and CRC1243 (A12). L.G. & O.W. received funding from CWCUK (grant 14-169) and GOSHCC (grant V2617). A.E. receives research grants from the Austrian Science Fund (FWF; Transcan I2795-B28 to A.E. (FIRE-CLL), DACH grants I3282-B26 and I1299-B21 (FOR2036) and a grant from the Paracelsus Medical University (PMU Grant E-13/18/091-EGF). S.S. receives funding from the DFG (SFB1074 , project B1), relevant to this work.

AUTHOR CONTRIBUTION

E.P., J.C. and A.M. performed and analyzed experiments. S.F. analyzed all RNAseq and mass spectrometry data with support from J.R.B.. A.S. performed and analyzed HSC and progenitor populations in KO and WT mice (fig.S2). M.M., in collaboration with J.C.W. and P.J.L., performed the PMP experiment. H.S., A.E. and M.S.S. contributed conceptually to the project. V.E. and M.B. performed ALL-PDX experiments. Additionally, L.G. and O.W. made a substantial contribution to carrying out the ALL-PDX studies and helped critique the output for important intellectual content. J.B. and S.S. provided data depicted in Fig. 3J and K; fig. S6E. *Prkcb*-KO mice were provided by M.L.; The manuscript was written by E.P., M.S.S. and I.R.

COMPETING INTERESTS

The authors declare to have no conflicts of interest.

DATA AND MATERIAL AVAILABILITY

The authors declare that the data supporting the findings of this study are available within the paper and its supplementary information.

The gene expression profile data have been deposited in the GEO database under accession numbers GSE119808 (CLL RNA-Seq, Fig. 3) and GSE119813 (Stromal RNA-seq, Fig. 4).

<https://www.ncbi.nlm.nih.gov/geo/query/acc.cgi?acc=GSE119808>

<https://www.ncbi.nlm.nih.gov/geo/query/acc.cgi?acc=GSE119813>

The mass spectrometry proteomics data (Fig. 5) have been deposited to the ProteomeXchange Consortium via the PRIDE partner repository with the dataset identifier PXD011062 and 10.6019/PXD011062.

<https://www.ebi.ac.uk/pride/archive/projects/PXD011062>

All other remaining data are available within the Article and Supplementary Files, or available from the authors upon request

FIGURE LEGENDS

Fig. 1. Normal and malignant B1 cells require microenvironment PKC- β for survival

- A. Quantification of CFSE-labeled E μ -TCL1 cells as a percentage total CD19⁺ cells detected in respective tissues. Analyses are pooled from two independent experiments using two primary tumors.
- B. Ratios of mean percentage CFSE⁺ of CD19⁺ between Day 8 -14 to Day 2.
- C. Representative FACS histograms of various tissues, 2 and 14 days post-transplantation into respective PKC- β WT and KO mice. Mean fluorescence intensity (MFI) of CFSE staining in CD19⁺ cells are noted alongside respective histograms.
- D. Quantification of CFSE MFI in CD19⁺ E μ -TCL1 cells detected in bone marrow, spleen, and peritoneal cavity of PKC- β WT and KO mice. Analyses are pooled from two independent experiments using two primary tumors.
- E. An experimental schematic to assess the functional consequence of adoptive transfer of CD45⁺ selected PKC- β WT BM or KO BM, respectively, into lethally-irradiated (10 Gy) PKC- β WT or KO recipients.
- F. Non-irradiated WT control (n=3), *WT:KO* (n=7), and 4 individuals of *WT:WT*, *WT:KO*, and *KO:KO* were assessed for peritoneal CD19⁺CD5⁺IgM⁺ cells with the label of donor cells in bold. Statistical significance was assessed using unpaired, two-tail Student t-tests.
- G. Assessed levels of serum immunoglobulins 9 weeks post-transplantation are shown with individual values representing the mean of duplicate measurements. Cohort means are shown with \pm SEM.
- H. Schematic of secondary transplantation of E μ -TCL1 cells into PKC- β chimeras.
- I. Representative flow cytometry plots of CFSE detection and CD19 staining from the peripheral blood of chimeras receiving TCL1-transplants. Chimeras are labelled with genotype of donor cells italicized and recipient genotype also indicated.
- J. Quantification of CFSE-labelled CD19⁺ E μ -TCL1 cells as a percentage total CD19⁺ cells detected in the peripheral blood from E μ -TCL1 recipients.

Fig. 2. Stromal PKC- β confers drug resistance to malignant B cells via BCL- X_L expression

- A. Representative Annexin-V and DAPI stains of mono-cultured or respective co-cultured CLL cells, 72 hours post-seeding of CLL.
- B. Percentage of Live (Annexin V⁻, DAPI⁺), Annexin-V⁺, and Dead (DAPI⁺Annexin-V⁺) stained cells are shown for individually cultured primary CLL (n=7 unique patients) for the three culture-conditions. Statistical significance for live cells between conditions was assessed, using paired, two-tail Student t-tests.
- C. IC₅₀ graphs of human CLL cells after 72 hours mono-culture, PKC- β WT co-culture or PKC- β KO co-culture, respectively, in the presence of venetoclax, bendamustine, fludarabine, ibrutinib or idelalisib treatment administered 24 hours post-seeding of CLL (n=5 patients per culture condition). CLL viabilities were normalized to respective DMSO controls. Statistical significance between PKC- β WT and PKC- β KO are shown.
- D. Annexin V⁻ measured viability of CLL cells (n=6) normalized to DMSO control, following 72 hours after PKC- β WT co-culture in the presence of increasing concentrations of enzastaurin, sotrastaurin, or midostaurin administered 24 hours post-seeding of CLL. Individual values from (b) are plotted for reference.
- E. Viability of CLL cells normalized to respective DMSO controls, following 72 hours PKC- β WT co-culture with 48 hours of exposure to increasing doses of venetoclax (n=9; n=21 at 5nM dose) or fludarabine (n=9; n=8 at 100 μ M dose) \pm enzastaurin treatment.
- F. Linked graphs of patient CLL cell viability (n=7), in the presence of labeled treatments co-cultured on PKC- β KO stroma. Statistical significance was assessed using ratio-paired, two-tail Student t-tests.
- G. Synergism was calculated using Combenefit Software (CRUK), within the Bliss model, for venetoclax combined with enzastaurin, sotrastaurin, or midostaurin, respectively (n=6). Heatmaps reflect assessment values noted for respective compound combinations, with error (\pm) indicated below. A scale of 50 to -50 is applied to values, with 50 representing maximal synergism and -50 being maximal antagonism. * $p < 5 \times 10^{-2}$; ** $p < 10^{-3}$; *** $p < 10^{-4}$
- H. BCL2 family proteins and β -Actin immunoblots of primary CLL at indicated time-points of venetoclax treatment, co-cultured with either PKC- β WT stroma or PKC- β KO stroma.
- I. BCL2 family proteins and β -Actin immunoblots of primary CLL at indicated time-points of venetoclax, fludarabine, or bendamustine treatment, co-cultured with PKC- β WT stroma \pm enzastaurin.

Fig. 3. Stromal PKC- β is essential for PI3K- and ERK-activation in CLL cells.

- A. Heat map of genes from co-cultured CLL cells after 24 hours of treatment. Purified CLL cells were harvested prior to RNA isolation (stroma contamination <1%). cDNA libraries were generated from purified mRNA, and sequencing was performed on Illumina's HiSeq 4000 to generate 50 bp single end (SE) reads. Unsupervised hierarchical clustering show genes that are differentially expressed in co-culture with either PKC- β WT stroma or PKC- β KO stroma, respectively, under vehicle treatment (left half of the map) or venetoclax treatment (right half of the map). Red and blue indicate relative high and low expression, respectively. Each condition analyzed depict three unique primary CLL samples.
- B. GSEA analysis evaluating canonical pathways enriched in CLL cells co-cultured with PKC- β WT stroma.
- C. IPA (Qiagen NV) analysis of predicted upstream regulators of observed differential CLL expression based on computed activation z-score.
- D. BCL-X_L, phosphorylated ERK (Thr202/Thr204), total ERK, phosphorylated JNK (Thr183/Thr185), phosphorylated p38 (Thr180/Tyr182) and β -Actin immunoblots of primary CLL at indicated time-points of venetoclax treatment, co-cultured with either PKC- β WT stroma or PKC- β KO stroma.
- E. BCL-X_L, phosphorylated ERK (Thr202/Thr204), total ERK and β -Actin immunoblots of primary CLL under venetoclax treatment co-cultured with PKC- β WT stroma \pm trametinib (1 μ M).
- F. Viability of CLL cells (n=9) following 72 hours PKC- β WT co-culture with 48 hours of exposure to venetoclax \pm trametinib treatment. Annexin V measured viability of CLL cells normalized to DMSO controls. Statistical significance was assessed using a paired two-tail Student t-test.
- G. Annexin-V measured CLL cell viability (n=5) following 72 hours PKC- β WT co-culture with 48 hours of exposure to venetoclax \pm idelalisib treatment or \pm enzastaurin treatment.
- H. Total AKT, phosphorylated AKT (T308), phosphorylated AKT (S473) and β -Actin immunoblots of primary CLL under venetoclax treatment co-cultured with PKC- β WT stroma \pm idelalisib (7.5 μ M).
- I. Total AKT, phosphorylated AKT (T308), phosphorylated AKT (S473), BCL-X_L, and β -Actin immunoblots of primary CLL co-cultured with either PKC- β WT stroma or PKC- β KO stroma under venetoclax treatment.
- J. Heatmap displaying mRNA expression profiles of patient samples (n=51) after clustering of 6 CLL-genes regulated by microenvironmental PKC- β . Two major clusters, classified as gene signature "high co-expression" and "low co-expression", segregate the cohort.
- K. Kaplan-Meier curves (x-axis with time since treatment) according to respective clusters ("High co-expression" vs. "Low co-expression"), showing statistically significant differences (pairwise log-rank tests) for median overall survival (OS) ("High co-expression": 413 vs. "Low co-expression": 1319 days; p<0.004).

Fig. 4. PKC- β dependent lysosome biogenesis is central for stroma-mediated drug resistance.

- A. Differential gene expression between PKC- β WT and KO stroma co-cultured with patient CLL cells (n=3) for 48 hours. The differentially expressed genes encoding plasma membrane and intracellular vesicle proteins are highlighted in blue and red, respectively. Significantly deregulated genes (p -adj <0.05, fold-change >2; 3,352 genes) were compared to the lists of annotated gene-sets for plasma membrane proteins (Protein Atlas; 1,734 genes) or intracellular vesicle genes (Gene Ontology Consortium; 1,259 genes), respectively.
- B. GSEA analysis enrichment of canonical pathways associated with PKC- β WT stroma co-culture with patient CLL cells (n=3).
- C. Heatmap depicting differentially expressed genes between PKC- β WT and KO from a Lysosomal Biogenesis geneset (Reactome).
- D. LAMP-1, TFEB and β -Actin immunoblots of respective PKC- β WT stroma and PKC- β KO stroma, co-cultured with primary CLL under venetoclax treatment.
- E. Immunoblots of TFEB and TBP from respective nuclear lysates of PKC- β WT stroma and PKC- β KO stroma \pm primary CLL co-culture.
- F. Immunoblot of TFEB for *Tfeb*-deleted stroma(sgRNA_3) and sgRNA control stroma and β -Actin under CLL co-culture conditions.
- G. Linked viability plots of patient CLL cells (n=9) treated with vehicle or venetoclax under co-culture with PKC- β WT control or *Tfeb*-deleted stroma.
- H. CLL viability assay (n=5) following 72 hours PKC- β WT co-culture with 48 hours of exposure to enzastaurin, chloroquine, or bafilomycin \pm venetoclax treatment.
- I. Linked viability plots of patient CLL cells (n=10) treated with vehicle or venetoclax under the respective co-culture conditions. Statistical significance was assessed using paired, two-tail Student t-tests.
- J. Immunoblots of BCL-X_L, p-ERK, and β -Actin of CLL co-cultured on either PKC- β KO control or caTFEB transduced stroma \pm venetoclax treatment.
- K. TCL1-transplanted PKC- β WT recipients were treated with the indicated treatments 3 days post-transplantation for the duration of 3 days. Bone marrow was subsequently analyzed for Lamp-1 and Lamp-2 expression in viable MSCs (CD45⁻Ter119⁻, left graph) and non-MSCs (CD45⁺Ter119⁺, right graph), with representative flow cytometry gating shown. Mean fluorescence intensity (MFI) of Lamp-1 and Lamp-2 are depicted for individual mice in both graphs, with statistical significance determined using an unpaired two-tail Student T-test.

Fig. 5. Stroma PKC- β regulates plasma membrane integrity and VCAM1 expression

- A. Linked viability plots of CLL patient samples (n=11) \pm Transwell sequestration in the presence of PKC- β WT stroma, under respective vehicle or venetoclax treatment. CLL viabilities are normalized to respective DMSO controls.
- B. Global heatmap of plasma membrane proteins from PKC- β WT stroma \pm primary CLL co-culture, treated with either vehicle or enzastaurin (5 μ M), analyzed by mass spectrometry. The heatmap presents clustering of log₂-transformed plasma membrane protein abundance for each of three replicates (k-means clustering; k=5), while the side plot depicts the mean protein abundance value for each treatment condition (maximum value of 225).
- C. Heatmap of significantly altered plasma membrane proteins on the surface of PKC- β WT stroma co-cultured with CLL and treated with either vehicle or enzastaurin (5 μ M) (q-values <0.05).
- D. FACS histograms of Vcam1(CD106) expression on PKC- β WT and PKC- β KO stromal mono-cultures.
- E. Linked viability plots of CLL patient samples (n=10) normalized to respective DMSO controls, in the presence of PKC- β WT stroma \pm genetic deletion of Vcam1, under respective vehicle or venetoclax treatment.
- F. Linked viability plots of CLL patient samples (n=9) normalized to respective DMSO controls, in the presence of PKC- β WT stroma \pm Vcam1 neutralizing or control antibody, under respective vehicle or venetoclax treatment.
- G. FACS analysis of Vcam1 expression in CLL co-cultured on PKC- β WT stroma with Crispr-deleted cells transduced with sgRNA control or Tfeb-deleted stroma.
- H. FACS analysis of Vcam1 expression in PKC- β WT and transduced PKC- β KO stroma.
- I. Percentage plots of adhesion (blue) and mobilization (red) of CLL cells under the various indicated co-culture and treatment conditions.
- J. Experimental schematic to assess whether enzastaurin mobilizes CLL from leukemic E μ -TCL1 mice.
- K. Graph of CD19⁺CD5⁺ cells in the peripheral blood of vehicle-treated E μ -TCL1 (n=4), enzastaurin-treated mice (n=5), and non-leukemic controls (n=4).
- L. Graph of CD19⁺CD5⁺ cells in the various noted compartments of vehicle-treated E μ -TCL1 (n=4), enzastaurin-treated mice (n=5), and non-leukemic controls (n=4).
- M. Representative flow cytometry gating depicting bone marrow stromal cells (CD45⁻ Ter119⁻) assessed for Vcam1 expression in vivo.
- N. Representative FACS histograms of Vcam1 MFI from DAPI⁻CD45⁻Ter119⁻CD106⁺ cells from bone marrow of E μ -TCL1 and PKC- β KO mice.
- O. Graph of DAPI⁻CD45⁻Ter119⁻ CD106 MFI cells from bone marrow of indicated E μ -TCL1 mice treated with vehicle (n=4), treated with enzastaurin (n=5), and PKC- β KO mice (n=4).

Fig. 6. Enzastaurin enhances the therapeutic effects of chemotherapy *in vivo*

- A. Graphs of E μ -TCL1 CLL cells (CD5⁺B220⁺) in peripheral blood from treatment cohorts for the indicated post-transplantation timepoints.
- B. Kaplan–Meier survival curves of leukemic mice following vehicle therapy, respective single-agent therapies, and combined therapy of enzastaurin (60mg/kg) and venetoclax (100mg/kg) following IP injection of 2 respective E μ -TCL1 tumors. Statistical significance was determined using Log-rank (Mantel-Cox) analysis. Dosing scheme shown in fig. S9A.
- C. BCL-X_L expression measured by flow cytometry as MFI of CD19⁺ splenocytes isolated from TCL1-engrafted wild-type mice treated for 72 hours with either vehicle (n=6) or venetoclax (n=7).
- D. Kaplan–Meier survival curves of leukemic mice following respective single-agent fludarabine therapy, and combined therapy of enzastaurin (60 mg/kg) and fludarabine (34 mg/kg) following IP injection of 2 respective E μ -TCL1 tumors. Schematic of dosing shown in fig. S9E.
- E. PKC- β -deficient (KO) mice received transplants of E μ -TCL1-HG splenocytes. Respective treatments began 72 hours post-transplantation, continuing for 3 days. Statistical significance was determined using Log-rank (Mantel-Cox) analysis.
- F. Linked viability graphs of primary MCL cells, normalized to respective DMSO controls, following co-culture with 48 hours of exposure to indicated doses of venetoclax (n=9) \pm enzastaurin treatment. Statistical significance was assessed using a paired two-tail Student t-test.
- G. Linked viability graphs of primary ALL cells following 72 hours PKC- β WT co-culture with 48 hours of exposure to indicated doses of dexamethasone or vincristine (n=9) \pm enzastaurin treatment. ALL viabilities were normalized to respective DMSO controls.
- H. Linked viability graphs of ALL cells, normalized to respective DMSO controls, following 72 hours PKC- β KO co-culture with 48 hours of exposure to indicated doses of dexamethasone or vincristine (n=5) \pm enzastaurin treatment.
- I. Representative bioluminescent imaging of ALL-PDX engrafted NSG recipient mice from indicated treatment cohorts, 4 weeks post-transplantation.
- J. Kaplan-Meier curve of NSG engrafted ALL-PDX treatment cohorts from 3 independent experiments of 2 unique patient-derived xenografts (vehicle Control, MST= 69 days; enzastaurin-treated, MST= 69days; vincristine-treated, MST= 88 days; vincristine + enzastaurin-treated, MST= 101days).

Figure 1

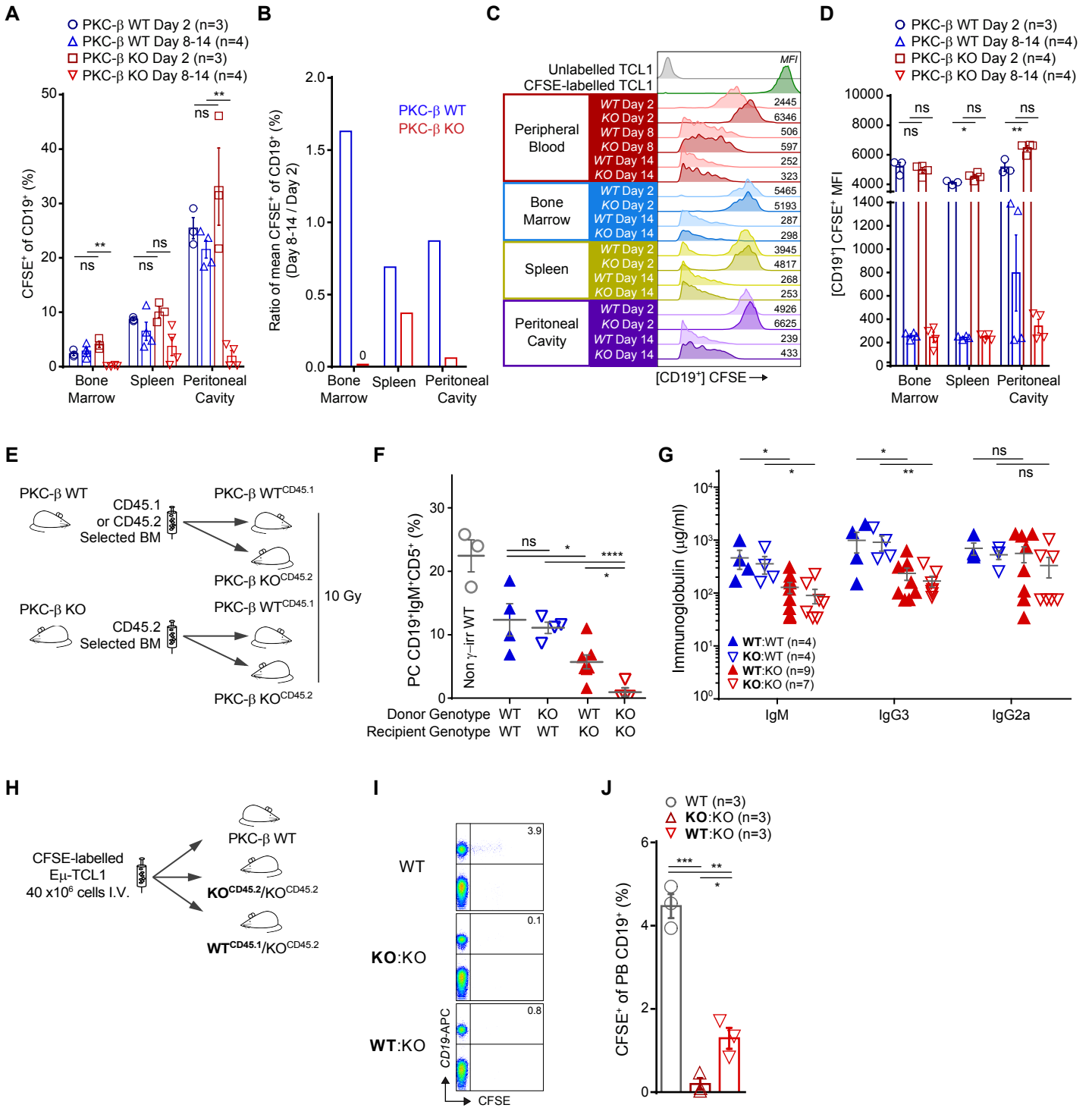


Figure 2

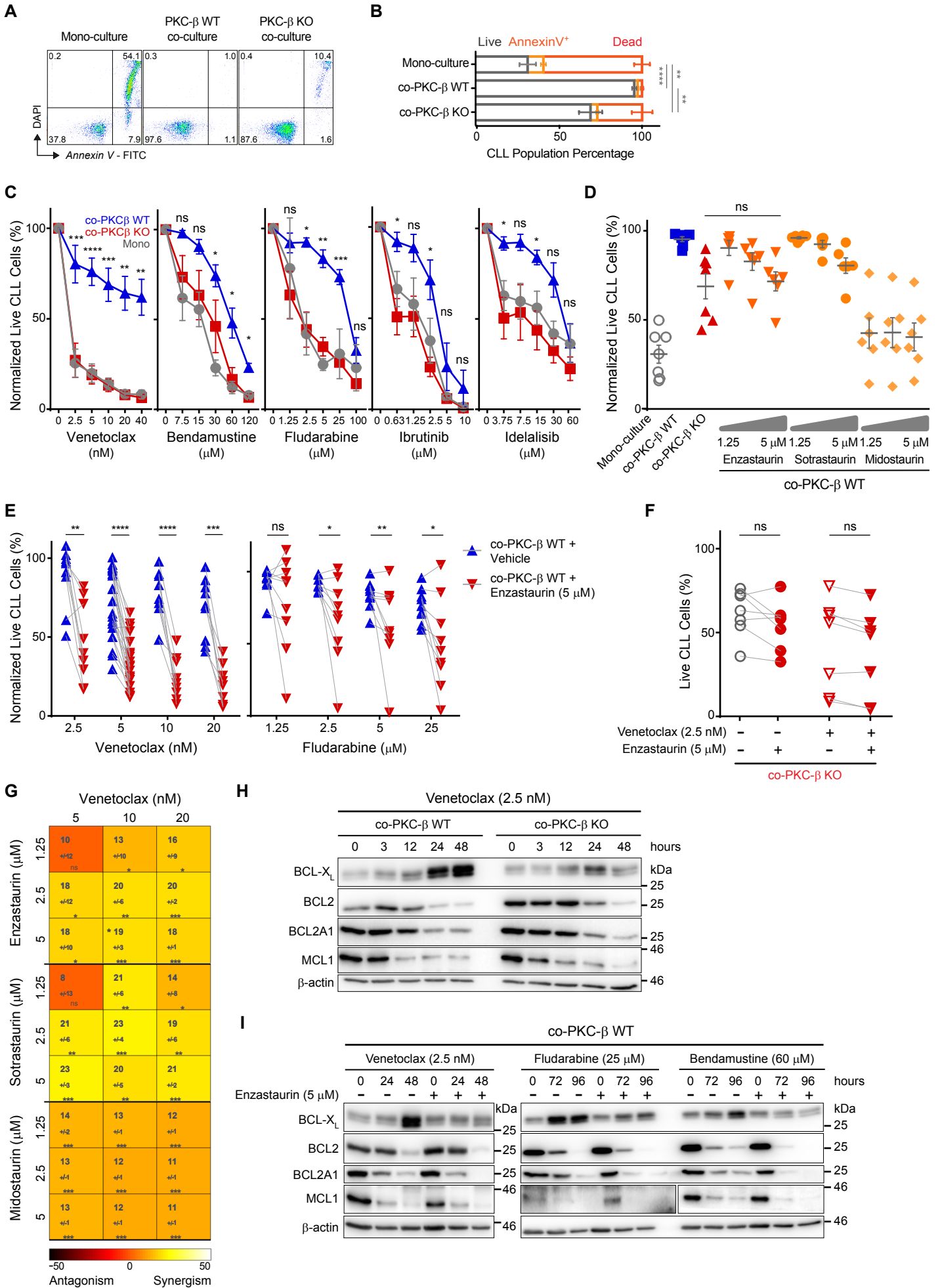


Figure 3

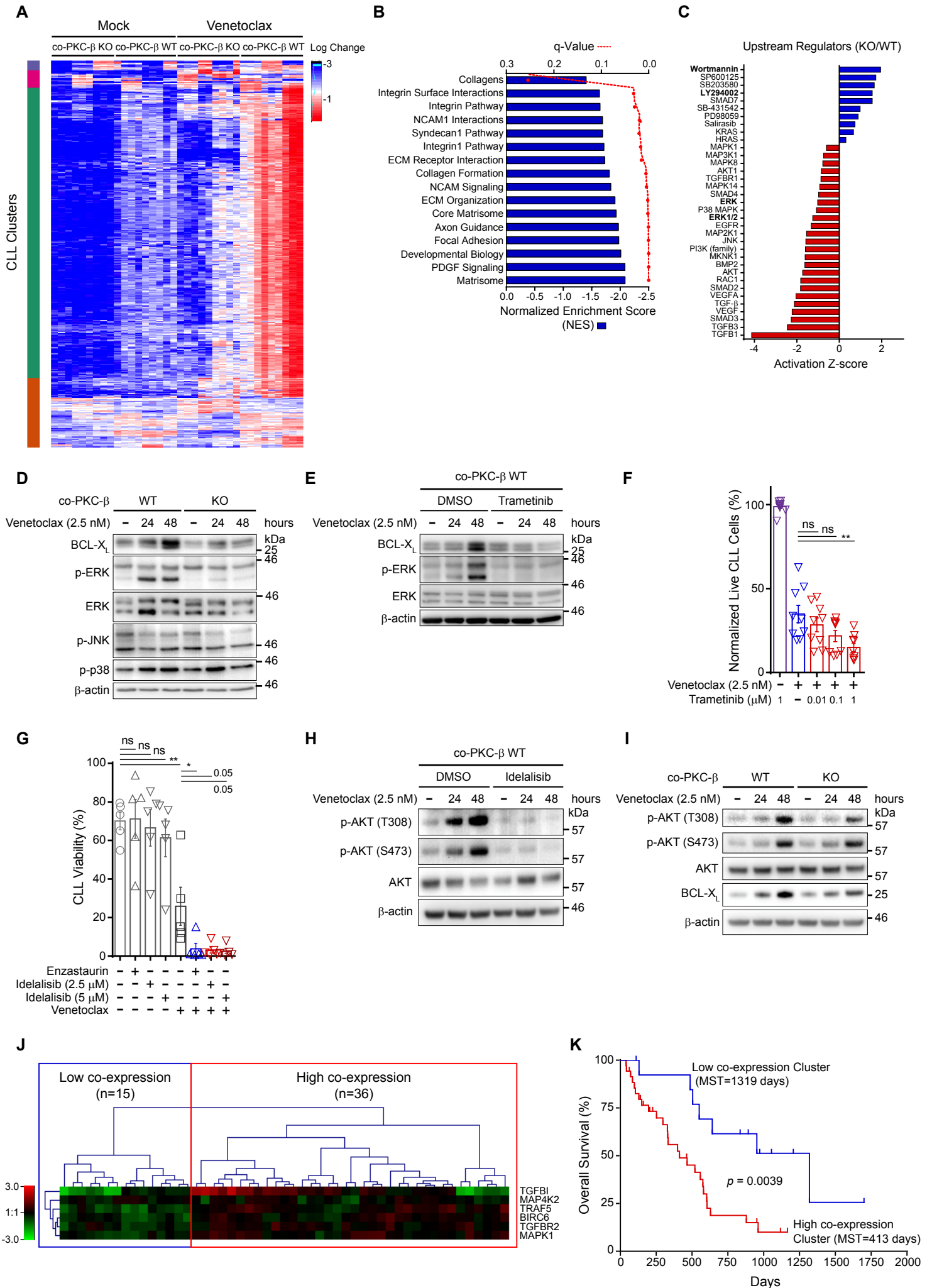


Figure 4

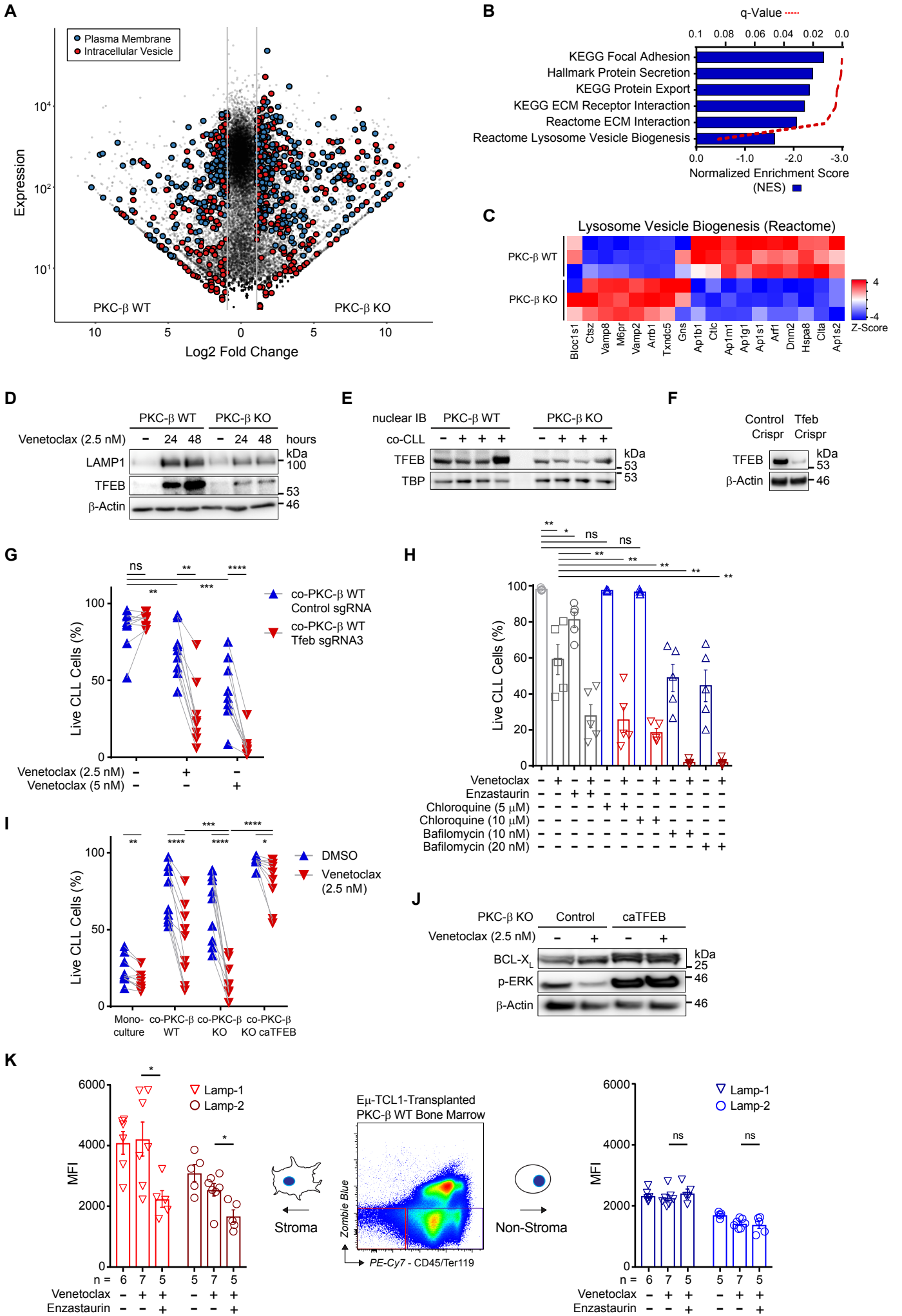


Figure 5

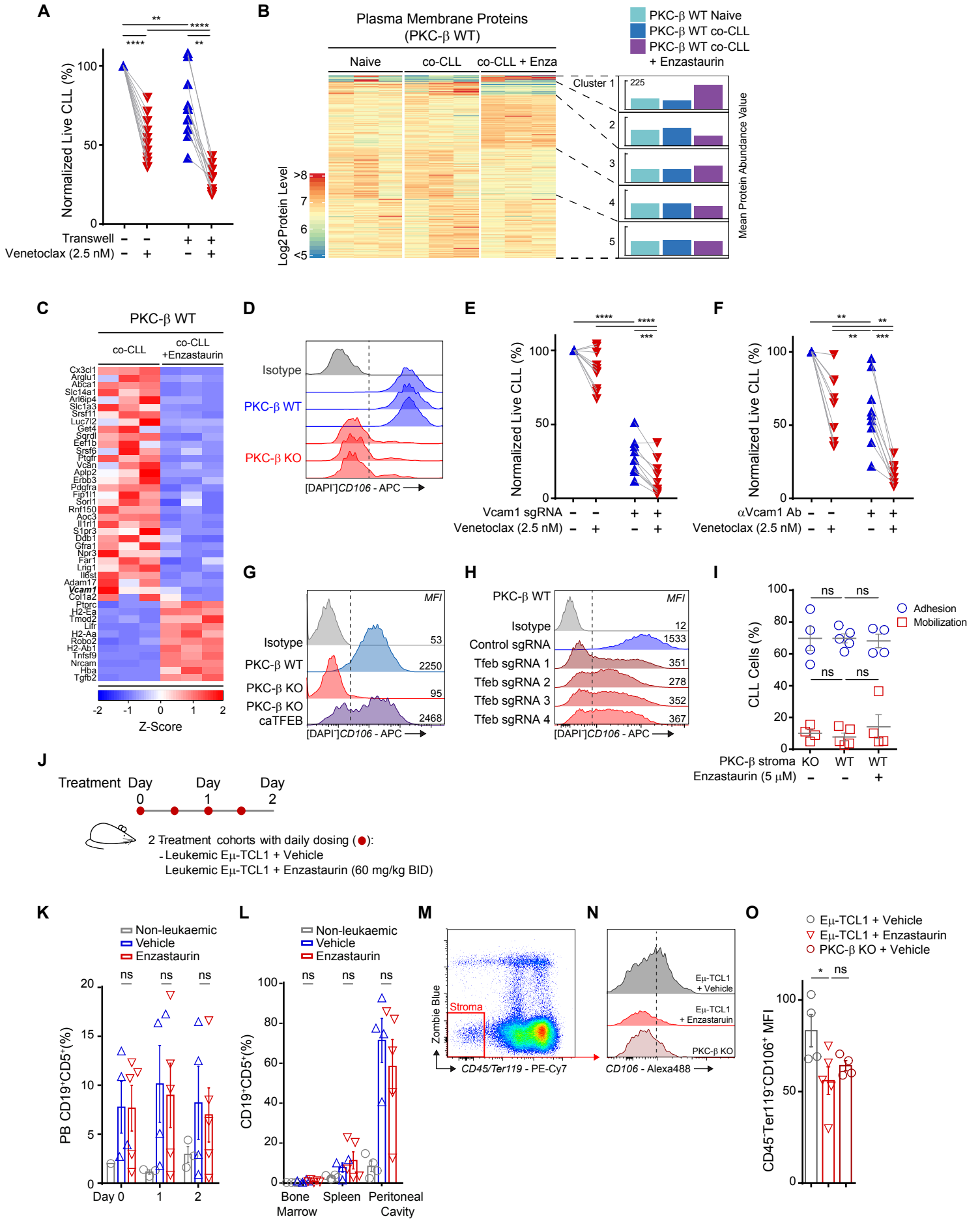


Figure 6

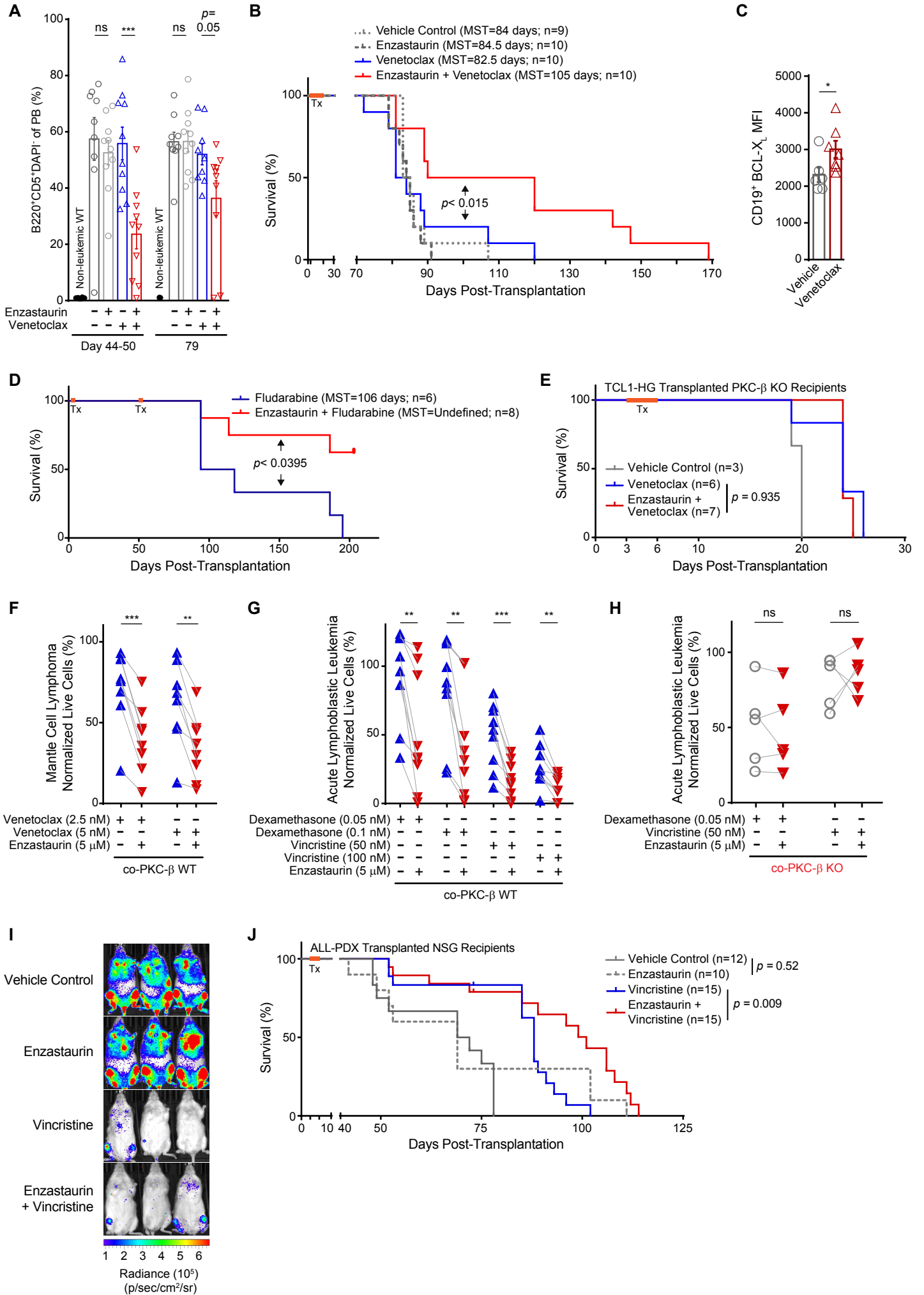
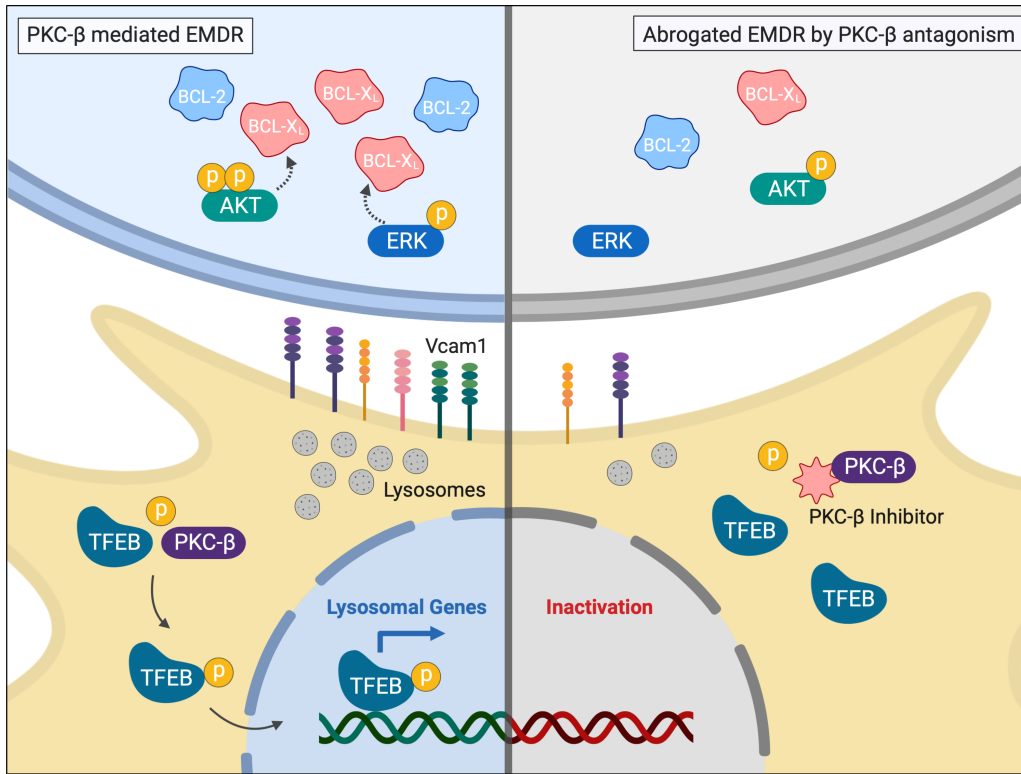


Figure 7



Supplementary Materials for

Stromal cell Protein kinase C- β inhibition enhances chemo-sensitivity in B cell malignancies and overcomes drug resistance

Eugene Park[‡], Jingyu Chen[‡], Andrew Moore[‡], Maurizio Mangolini, Antonella Santoro, Joseph R. Boyd, Hilde Schjerven, Veronika Ecker, Maike Buchner, James C. Williamson, Paul J. Lehner, Luca Gasparoli, Owen Williams, Johannes Bloehdorn, Stephan Stilgenbauer, Michael Leitges, Alexander Egle, Marc Schmidt-Supprian, Seth Frieze and Ingo Ringshausen*.

[‡] equal contribution

*Corresponding author. Email: ir279@cam.ac.uk

This file includes:

Materials and Methods

Fig. S1. Homing and engraftment kinetics of E μ -TCL1 CLL in PKC- β wild-type and null mice.

Fig. S2. PKC- β deficiency does not overtly alter hematopoiesis.

Fig. S3. PKC- β chimeras engraft with comparable efficiency irrespective of donor or recipient genotype.

Fig. S4. Monocytes confer CLL survival support but not PKC- β dependent EMDR, in contrast to MSCs.

Fig. S5. PKC- β -mediated EMDR involves increased protein levels of BCL-X_L.

Fig. S6. CLL signaling pathways regulated by stromal PKC- β correlate with clinical outcomes.

Fig. S7. Stromal lysosomes, and lysosomal biogenesis regulator TFEB, are central to PKC- β -mediated EMDR.

Fig. S8. PKC- β is dispensable for *in vitro* and *in vivo* mobilization of leukemia.

Fig. S9. *In vivo* co-targeting of PKC- β does not contribute to increased off-target cytotoxicity.

Fig. S10. EMDR derived from splenic stroma is mitigated by PKC- β antagonism.

Fig. S11. Representative FACS gating strategies.

Table S1. Patient characteristics

Table S2: Key reagents

Data File S1. Excel file of top deregulated genes from CLL RNA-Seq in Fig.3C.

Data File S2. Excel file of proteomic clusters from Fig. 5B,C.

Data File S3. Excel file of individual data from experiments with n<20 per group.

References (60–68)

Materials and Methods

Primary cells and cell culture

After informed patients' consent and in accordance with the Helsinki declaration, peripheral blood was obtained from patients with a diagnosis of CLL, ALL, or MCL. Studies were approved by the local ethical committees of the Cambridgeshire Research Ethics Committee (07/MRE05/44), Technical University Munich (project number 1894/07), and the Institutional Review Board of the Erasmus MC. Peripheral blood mononuclear cells (PBMC) were isolated from heparinized blood samples by centrifugation over a Ficoll-Hypaque layer (PAN-Biotech). Malignant B cells were harvested and cultured in RPMI 1640 (Gibco), supplemented with 10% fetal calf serum (FCS) penicillin/streptomycin 50 U/ml, sodium-pyruvate 1mM, L-glutamine 2 mM, L-asparagine 20 mg/ml, 50 μ M 2-mercaptoethanol, 10mM HEPES and MEM non-essential amino acids (Gibco). All primary mouse bone marrow stromal cell cultures were cultured in MEM Alpha + GlutaMAX medium (ThermoFisher Scientific) supplemented with 10% fetal calf serum, 10% horse Serum (StemCell Technologies) 10 μ M 2-mercaptoethanol and 1% penicillin/streptomycin (Gibco).

Extraction of murine bone marrow stroma cells

All *in vivo* experiments were conducted in accordance with UK Home Office regulations (License P846C00DB). Murine bone marrow MSCs were established from femora and tibiae of 4 to 8 week-old mice. Bone marrow stroma cells were harvested from young female age-matched *Prkcb*^{+/+} and *Prkcb*^{-/-} by flushing the cavities of femora and tibiae with PBS. After filtration through a 70- μ m filter and depletion of erythrocytes using a lysis buffer (BD PharmLyse; BD Biosciences), washed cells were either used further for experiments or cryopreserved.

Co-culture in vitro toxicity assay

Malignant B cells from CLL, ALL, or MCL patients co-cultured on murine BMSCs, CD14⁺, or splenic follicular reticular cells (FRCs; gp38⁺CD31⁻) from PKC- β WT or PKC- β KO mice. **Since PKC- β KO stroma grow marginally slower than WT, cell numbers were adjusted and BMSCs were seeded at equal concentrations of 2×10^4 cells per well of a 96-well plate and incubated for 24 hours to allow for attachment.** Subsequently, CLL, ALL, or

MCL cells were seeded at 2×10^5 cells per well for monoculture and co-culture conditions and incubated for 24 hours. Enzastaurin (Sigma-Aldrich), sotrastaurin, bendamustine, idelalisib, midostaurin (Selleck Chemicals), venetoclax (LC Labs), fludarabine (Cayman Chemicals), ibrutinib (SYNkinase), dexamethasone, and vincristine sulfate (Sigma-Aldrich) were added at specified concentrations and incubated for up to 48 hours, prior to flow cytometric analysis (representative gating depicted in fig. S11A).

Generation of chimeric mice

Bone marrow from CD45.2⁺ *Prkcb*^{+/+}, *Prkcb*^{-/-}, and CD45.1⁺ B6.SJL-Ptprca Pepcb/BoyJ (Jackson Laboratories) age-matched mice were isolated and depleted of CD45⁻ cells with purity of >95% confirmed by flow cytometry (muCD45 microbeads; Miltenyi Biotec). 3×10^6 cells of purified bone marrow of respective CD45.2⁺ *Prkcb*^{-/-} purified-BM and CD45.1⁺ B6.SJL-Ptprca Pepcb/BoyJ purified-BM were injected intravenously into respectively different CD45 recipients, post-irradiation (10 Gy) (i.e. CD45.1⁺ BM into CD45.2 recipient and CD45.2⁺ BM into CD45.1 recipient). CD45.2⁺ *Prkcb*^{-/-} BM was also injected into irradiated CD45.2⁺ *Prkcb*^{-/-} recipients as a control (Fig. 2). Chimerism was assessed by flow cytometry of CD45.1 and CD45.2 staining of peripheral blood withdrawn by tail vein bleeding (representative gating depicted in fig. S11B). Serum immunoglobulin isotype levels were assessed from peripheral blood using a mouse specific immunoglobulin isotype panel and subsequently analyzed and quantified using commercial software (LegendPlex Mouse Ig Panel, LegendPlex Analysis Software; Biolegend). Peritoneal fluid, peripheral blood, bone marrow, and spleen were harvested from respective animals and analyzed by flow cytometry. Chimeric mice of appropriate genotype upon confirmation of chimerism were injected with 40×10^6 CFSE-labelled *TCL1*-tumor cells intravenously and 1×10^6 cells injected intraperitoneally. Assessment of labeled CLL cells in peripheral blood was performed by flow cytometry.

Western blotting

After the specified time CLL cells were lysed in RIPA buffer and a total of 15 µg protein was separated by SDS-polyacrylamide gel electrophoresis, blotted to polyvinylidene difluoride (PVDF) membranes (Millipore) and probed with primary antibodies against BCL-X_L (Cell Signalling Technologies), BCL-2A1, β-actin (both Sigma-Aldrich), NOXA,

PUMA (both Abcam), BCL-2, BIM (both BD Biosciences), Mcl-1 (Santa Cruz Biotechnology).

RNA-sequencing and data analysis

CLL cells were cultured in mono-culture, or co-culture on murine BMSCs from WT or PKC- β KO mice for 12 hours. Primary CLL cells were seeded at 6×10^6 cells on the top of 1×10^5 bone marrow MSCs per well of a 6 well plate. CLL cells were harvested for bulk RNA extraction and DNase treatment (RNA mini-prep kit, Sigma-Aldrich). Purity was confirmed by FACS analysis to be >95%. Human CLL cDNA libraries were prepared by using NEBNext Ultra Directional RNA Library Prep Kit for Illumina (New England Biolabs). Quality of cDNA libraries were determined using a Bioanalyzer High Sensitivity Chip (Agilent). Single-read sequencing was performed on the Illumina HiSeq 4000 platform at the CRUK Cambridge Institute Genomic Core. Stromal cDNA libraries were similarly synthesized and analyzed.

Sequencing data quality was assessed using the RSeQC package(60) and low quality reads and adapter sequences were removed using Trimgalore. Filtered data were aligned to the mm10 or hg38 reference genomes using RNA-STAR aligner(61) using the GENCODE Release 25 comprehensive GTF file with the following parameters: --outSAMtype BAM SortedByCoordinate --sjdbGTFfile annotation.gtf --outFilterType BySJout --outFilterMultimapNmax 50 --alignSJoverhangMin 1 --outFilterMismatchNmax 2 --outFilterMismatchNoverLmax 0.04 --alignIntronMin 20 --alignIntronMax 1000000 --alignMatesGapMax 1000000 --outSAMstrandField intronMotif. Quantification of gene expression was performed with HTSeq-0.11.0 (62) against the comprehensive gene annotation files from GENCODE (m14 and v25, for mouse and human genomes, respectively). Differential expression analysis was performed using DESeq2(63), controlling for differences between patient samples. To generate the heat-map shown in Fig. 3, a matrix of normalized counts was constructed using all differentially expressed genes ($p_{adj} < 0.05$; LFC >2) from pairwise comparisons between conditions ($n=2,660$ genes) and k-means clustering of rows was performed ($k=4$).

Multivariate analysis of clinical data

For cross-validation of CLL-RNA sequencing analysis obtained (Fig. 3A-C, fig. S6A), we assessed the clinical impact of stromal PKC- β dependent gene expression through data generated from PBMCs derived from a cohort of fludarabine-resistant CLL patients (n=51) subsequently treated with subcutaneous Alemtuzumab in a multicenter phase 2 trial(23), (NCT00274976). Patient sampling was performed at enrollment and prior to Alemtuzumab treatment. Profiled mRNA was extracted using the Allprep DNA/RNA mini kit (Qiagen) on PBMCs purified using ficoll density gradient centrifugation. Quality control on purity, concentration and RNA integrity was assessed using the Agilent 2100 Bioanalyzer with the RNA 6000 Nano LabChip (Agilent Technologies) and the 2100 Expert Software. Samples used had an RNA Integrity Number (RIN) \geq 7.0. Affymetrix GeneChip® Human Exon 1.0 ST Array (Affymetrix) were used for expression profiling. Per sample, 250 ng RNA were amplified, transcribed to cDNA, fragmented and subsequently labeled with biotin. Array hybridization was performed at 45°C for 16-18h in the Affymetrix GeneChip Hybridization Oven 640, arrays were subsequently washed in the Fluidics Station 450 and scanned with the GeneChip scanner 3000 7G. Experiments were conducted according to the manufacturer's protocol.

Raw Affymetrix Human Exon array (HuEx-1_0-st-v2) data files were preprocessed by the robust multichip average (RMA) algorithm using Aroma. Affymetrix gene expression values were summarized on the transcript level using the 'core' probe set definition according to Affymetrix. The Genesis platform(64) was used for clustering. Respective cluster and survival analysis was conducted only for genes impacting survival and showing co-expression. Hierarchical clustering was used with Manhattan distance and complete linkage. Clinical endpoints used for the survival analysis were progression-free survival (PFS) and overall survival (OS), data was missing in 2 patients.

Plasma membrane profiling

Plasma membrane profiling was performed as described previously (65). Peptides were subsequently labelled with TMT reagents (Thermo Fisher Scientific), pooled and cleaned up using a SEP-PAK C18 cartridge (Waters) prior to high pH RP fractionation as previously described(66). High pH fractions were pooled orthogonally into 12 samples for analysis by LC-MS on an Orbitrap Fusion (Thermo Fisher Scientific) utilising synchronous

precursor selection mode to isolate reporter ions essentially as previously described(8). Data were searched using the MASCOT (Matrix Science, UK) search node within Proteome Discoverer v2.1 (Thermo Fisher Scientific). The database used was the SwissProt Mouse Reference Proteome including an appended database of common contaminants. Statistical differences between replicate groups were assessed using an implementation of LIMMA within the R environment including Benjamini-Hochberg correction for multiple hypothesis testing. The resulting p/q-values are reported. Experiment was performed in triplicate using one patient sample. For the heat-map shown in Fig. 5C, a matrix was constructed of the log₂ transformed abundance values with the addition of a pseudo-count of 8 for all mid- to high-confidence protein measurements. This matrix was then used for k-means clustering (k=5) for each replicate across each condition. The side plot of the figure was generated using the median value of the abundance values for each replicate. The plot was generated using the seqsetvis R package (Boyd J (2018)) including Benjamini-Hochberg correction for multiple hypothesis testing.

Flow cytometry

All antibodies for flow cytometry measurements, as well as their respective isotype controls, were obtained either from BD Biosciences, Biolegend, eBioscience, Tonbo Biosciences, or Santa Cruz Biotechnology. For apoptosis analyses, FITC-Annexin V and DAPI (Biolegend) were used. A complete list of all antibodies used for this study can be found in the supplementary information (table S2).

CRISPR/Cas9-mediated gene deletions

Single-guide RNA (sgRNA) sequences were cloned into lentiCRISPRv2. Control_sgRNA (TCGGCACTGGCGATCGGTTG), Vcam1_sgRNA (GCTGGAACGAAGTATCCACG), Tfeb_sgRNA_1 (TGGACACGTAAGTCCACCT), Tfeb_sgRNA_2 (CTGTAGTTGAGAGAAGACGC), Tfeb_sgRNA_3 (TGAGATGCAGATGCCTAACA), Tfeb_sgRNA_4 (CCTCTGTGGATTACATCCGG). Lentiviral infections of murine bone marrow stromal cells with the specific sgRNA constructs were performed. Following 48 hours of puromycin selection (2 µg/ml), cells were negatively sorted for Vcam1 expression and cultured for further experiments, while *Tfeb*-deleted stroma were left unsorted after 72 hours of puromycin selection (2 µg/ml).

Neutralizing antibody assay

Bone marrow MSCs were seeded at a concentration of 1×10^4 cells per well of a 96-well plate and incubated for 24 hours. Prior to addition of CLL cells 10mg/ml of neutralizing or control antibody, α VCAM1 and Control Rat IgG2a (both Biolegend), was added for 1 hour. CLL cells were then seeded at 2×10^5 cells per well for monoculture and co-culture conditions. Neutralizing antibodies were restored to 10 mg/ml following the addition of CLL cells. After 24 hours venetoclax was administered at 2.5 nM and incubated for a further 48 hours before flow cytometric analysis.

Ibidi flow chamber cell adhesion assay

Stromal cells of respective genotype, *Prkcb*^{+/+} and *Prkcb*^{-/-}, were seeded at a concentration of 3×10^4 cells/100 μ l into the channel of Ibidi channel tissue-culture treated μ -slides (Ibidi; type 1, 0.4 mm). 12 hours later fresh media was added simultaneously to both reservoirs. Primary CFSE-labeled CLL cells were counted by two individuals using trypan blue staining. The average of both counts determined the respective seeding cell numbers of each patient. After simultaneous removal of all reservoir media from channel slides, 500 μ l of patient cell suspension was placed in one of the experiment-long designated influx reservoirs. Flow-through from atmospheric pressure into the efflux reservoir was reapplied to the designated influx reservoir 3 times for each slide. Final flow-through from efflux reservoirs were counted twice for each slide, averaged, and subtracted from respective seeding cell counts for each patient to obtain percent adhesion. Subsequently, 300 μ l of media was placed into both reservoirs simultaneously and incubated for 24 hours. Cells were then exposed to respective treatments after simultaneously withdrawal of culture media, and simultaneous application of treatment media. 48 hours later, flow-through using 500 μ l of fresh media placed into the designated influx reservoirs were performed 3 times using fresh media each flow-through. Pass-throughs from the efflux reservoirs were collected and counted twice for cells, averaged and subtracted from each slide-specific number of adhered cells.

Generation of *Prkcb*^{-/-} stroma expressing constitutively active TFEB (caTFEB)

Plasmids pCIP-caHuTFEB and empty vector pCIP (Plasmids #79013,79009; Addgene) were linearized using Scal-HF restriction enzyme (New England Biolabs) (Young, NP 2016), and subsequently purified using a NucleoSpin Gel Purification Kit (Machery-Nagel). Transfections of a parental PKC- β KO stroma were performed, using 5.0 μ g of each respective linearized plasmid prepared with Lipofectamine 2000 transfection reagent (ThermoFisher Scientific). 48 hours post-transfection, transfected cells and untransfected control were cultured in stromal media (MEM + 10% FBS +10% Horse Serum) containing 2 μ g/ml of puromycin for 72 hours (ThermoFisher Scientific).

In vivo models for CLL homing and engraftment

For CLL homing experiments primary E μ -TCL1 tumor cells were labelled with 5 μ M Carboxyfluorescein-succinimidyl-ester (CFSE; Life Technologies) per manufacturer's protocol. Post-confirmation of labeling by flow cytometry, 40*10⁶ cells were injected intravenously, and 1*10⁶ cells injected intraperitoneally into age-matched mice of two genotypes. Peripheral blood was drawn by tail vein bleeding, and analyzed by flow cytometry following erythrocyte depletion.

In vivo model for Vcam1 biomarker \pm enzastaurin

Leukemic E μ -TCL1 mice were analyzed for leukemic burden by CD5⁺C19⁺ staining of peripheral blood. Cohorts were assembled to match overall leukemic burden of vehicle control between enzastaurin treatment cohorts. Enzastaurin or vehicle (5% dextrose + 10% ethanol in water), was administered at a dose of 60mg/kg BID for a total of 96 hours. Analyses of bone marrow Vcam1 expression was conducted 3 hours following last treatment, by flow cytometry. In brief, stromal cell populations were isolated from femur and tibia, crushed in mortar and pestle, and digested with 2 ml of collagenase I (Stem Cell Technologies) and 1 mg/ml collagenase IV (Sigma-Aldrich,) at 37°C in strong agitation for 30 minutes. Cells were washed with PBS + 2% FBS and filtered through a 40 μ m mesh filter. Red blood cells were lysed with Pharmalyse (BD Biosciences) for 10 minutes on ice. Aliquots from individual mice were analysed by flow cytometry (representative gating depicted in fig. S11C).

In vivo model for Lamp-1 and Lamp-2 biomarkers ± enzastaurin

72 hours post-transplantation TCL1-transplanted PKC-β WT recipients were treated with either vehicle, venetoclax (100 mg/kg per day), or pre-treated with enzastaurin (60 mg/kg BID) and concomitantly administered with enzastaurin + venetoclax for the duration of 3 days. Bone marrow was harvested 3 hours after administration of final dosing and subsequently analyzed for respective intracellular Lamp-1 and Lamp-2 expression after surface staining and subsequent fixation and permeabilization (Biolegend). Mean fluorescence intensities (MFIs) of Lamp-1 and Lamp-2 were assessed in viable MSCs (CD45⁻Ter119⁻) and non-MSCs (CD45⁺Ter119⁺). Statistical significance of intracellular staining was determined using an unpaired two-tail Student T-test.

In vivo CLL study of venetoclax ± enzastaurin

C57B/6J mice (Jackson Labs) were injected intraperitoneally with either 3.5×10^6 or 5×10^6 cells of two respective primary E μ -TCL1 tumors. 72 hours post-transplantation respective treatments began by oral gavage for 16 consecutive days. Venetoclax was solubilized as previously reported (67). In brief, venetoclax was formulated in phosal-50 propylene glycol (60%), polyethyleneglycol-400 (30%), and ethanol (10%). Leukemic burden was assessed by erythrocyte-depleted peripheral blood analyzed by flow cytometry.

In vivo CLL study of fludarabine ± enzastaurin

C57B/6J (Jackson Labs, UK) mice were injected intraperitoneally with 5×10^6 cells of two respective primary E μ -TCL1 tumors. 72 hours post-transplantation mice respective treatments began by oral gavage and intraperitoneal injection. Fludarabine phosphate (Sigma-Aldrich) was solubilized in sterile PBS. Mice received Fludarabine treatment for 5 consecutive days for two cycles. Enzastaurin or vehicle was administered twice daily of the same periods. Leukemic burden was assessed by peripheral blood analyzed by flow cytometry.

In vivo ALL-PDX study of vincristine ± enzastaurin

NOD.*Cg-Prkdc^{scid}Il2rg^{tm1Wjl}*/SzJ (NSG) mice were injected intravenously with $2-3 \times 10^5$ cells of luciferase-transduced ALL xenografts cells derived from 2 unique patient samples. In 3

independent experiments, cohorts were respectively treated 72 hours post-transplantation. enzastaurin (60mg/kg BID) or vehicle control was administered orally, 12 hours prior to intraperitoneal dosing of vincristine or vehicle and continued for 72 hours thereafter. Vincristine (Sigma-Aldrich) was solubilized in sterile PBS and administered once per treatment cycle at a weight-adjusted dose between 0.5 mg/kg and 0.6 mg/kg (68). Animals received equal treatment dosages between treated cohorts for each independent experiment, for one or two cycles. For the combination treated cohorts, 14 mice received one-cycle, whereas 5 mice received a second treatment cycle 4 weeks following initial treatment. Anesthesia-related morbidities on Day 73 post-transplantation in one independent experiment resulted in the censoring of 3 (vincristine) and 4 (combination treatment) animals. Leukemic burden was assessed by peripheral blood, which was analyzed by flow cytometry and by bioluminescent imaging (Xenogen IVIS). Luciferin was administered intraperitoneally to anesthetized animals prior to live imaging.

Statistical analysis

Statistical analyses of results were performed using one-way ANOVA followed by two-tail Student t-tests, with respective unpaired and paired analyses experimentally dependent. Statistical annotations as previously noted were denoted with asterisks according to the following, **** $p < 0.0001$, *** $p < 0.001$, ** $p < 0.01$, * $p < 0.05$, and ^{ns} $p > 0.05$.

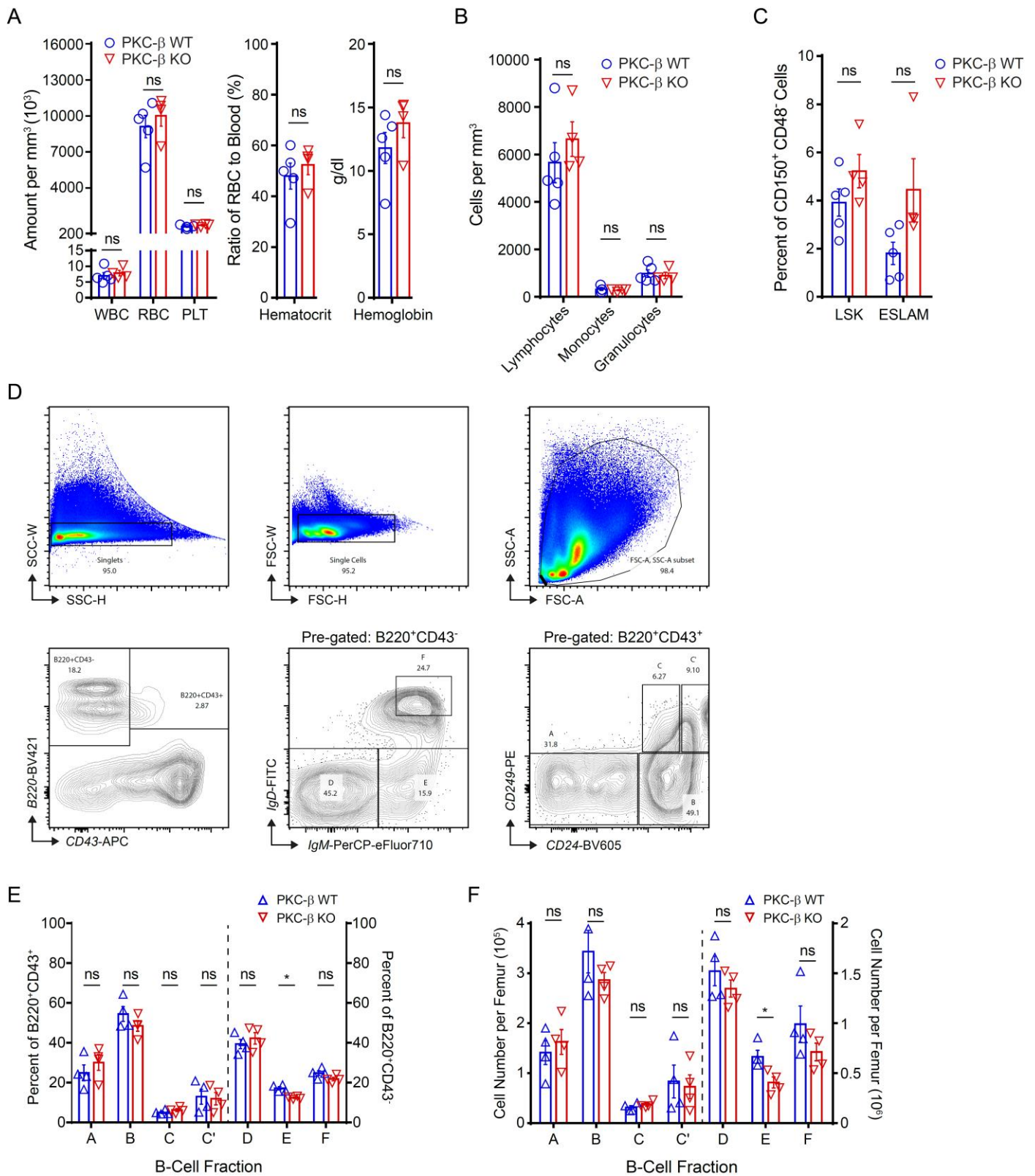


Fig. S2. PKC- β deficiency does not overtly alter hematopoiesis. (A) White blood cell (WBC), red blood cell (RBC), and platelet (PLT) abundance are shown from complete blood counts of peripheral blood from age-matched PKC- β WT and KO mice. **(B)** Individual abundance of white blood cell types is graphically shown. **(C)** Bone marrow composition of Lin⁻Sca1⁺C-Kit⁺ (LSK) and CD150⁺CD48⁺CD45⁺EPCR⁺ (ESLAM) hematopoietic stem cells are shown as a percentage of CD150⁺CD48⁺ cells. **(D)** Representative gating strategy of bone marrow B-cell progenitors. **(E)** Composition of B-cell

progenitor fractions (Hardy fractions) are shown as a percentage of B220⁺CD43⁺ (left axis, Fraction A-C') and of B220⁺CD43⁻ (right axis, Fraction D-F). **(F)** Absolute numbers of B-cell progenitor fractions (Hardy fractions) are shown as a total of RBC-lysed bone marrow from a respective femur of PKC-β WT (n=4) and KO (n=4) mice (left axis, Fractions A-C'; right axis, Fraction D-F).

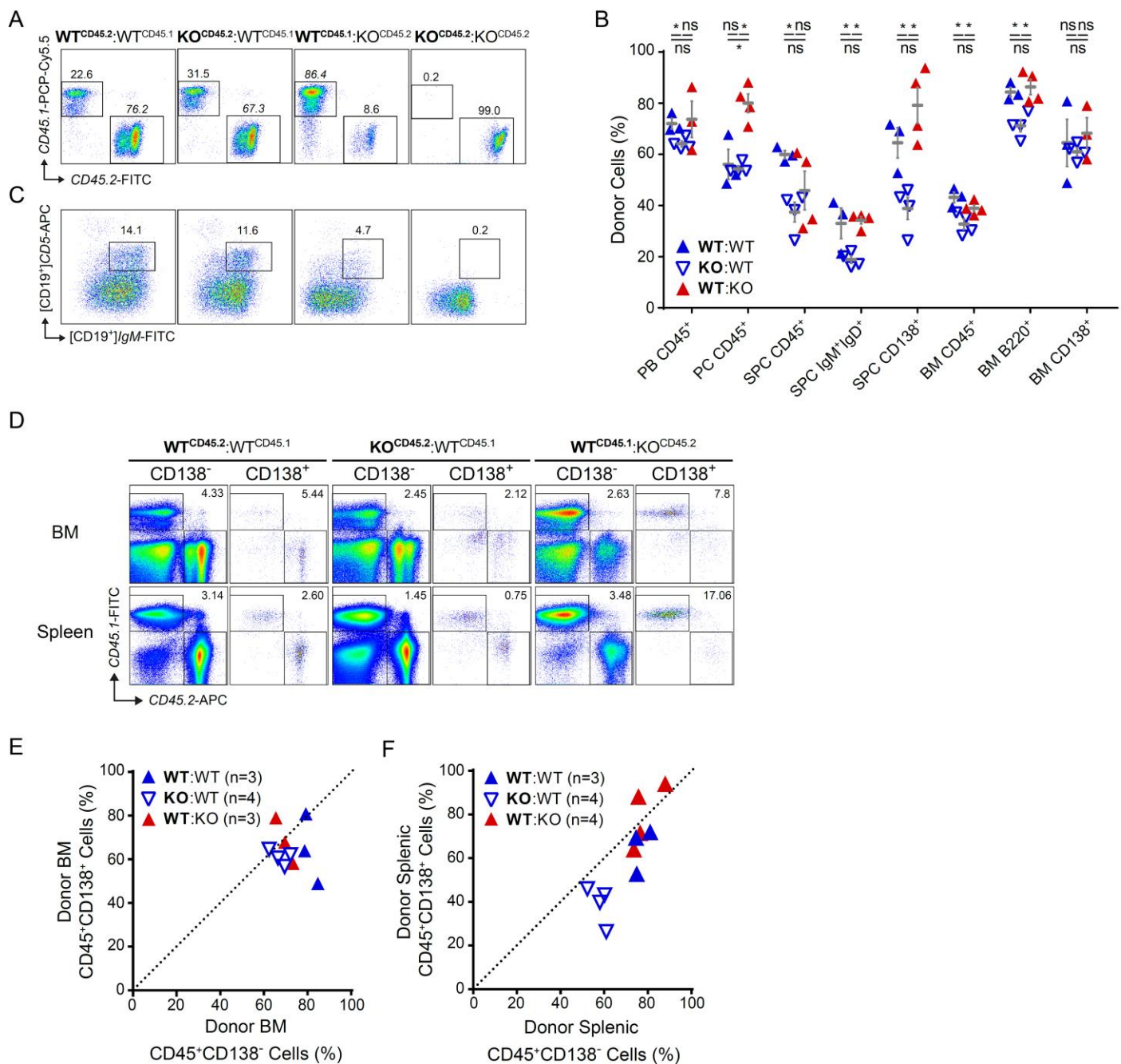


Fig. S3. PKC- β chimeras engraft with comparable efficiency irrespective of donor or recipient genotype. (A) Representative CD45.1 and CD45.2 FACS plot stains of peripheral blood, 8 weeks post-transplantation, are shown with the donor label and percentage of donor cells denoted in bold. **(B)** Representative CD5 and IgM FACS plots for CD19⁺ cells of the peritoneal cavity are shown for the similarly labeled cohorts as above in fig. S3A. **(C)** Assessment of chimerism in mice with mismatched CD45 isotypes. Percentages of respective donor CD45 isotype are shown \pm SEM. Genotype of donor BM is set in bold; **WT:WT** (n=3), **KO:WT** (n=4), and **WT:KO** (n=4; n=3 for PB CD45⁺ and BM CD138⁺). Abbreviations for tissues as follows: PB, peripheral blood; PC, peritoneal cavity; SPC, splenocytes; BM, bone marrow. Ten weeks post transplantation, a mixed chimerism was observed in the peripheral blood with a predominance of the transplanted bone marrow cells (**WT**(donor):**WT**(recipient)=72.0% \pm 2.09%, **WT:KO**=73.7 \pm 7.11%, **KO:WT**=64.1% \pm 1.13%). **(D)** Representative CD45.1⁺ and CD45.2⁺ stains of respective CD138⁻ and CD138⁺ BM or splenic cells are shown. Ratios of donor : recipient are indicated within respective stains. **(E)** Graphs of percent donor BM CD45⁺CD138⁺ cells and percent donor BM CD45⁺CD138⁻ cells are plotted, with equal donor engraftment of both \pm CD138 compartments depicted by the dotted line. Percentages of donor cells are shown as a subset of total CD45⁺ cells. **(F)** Graphs of splenic donor CD45⁺CD138⁻ engraftment and splenic donor CD45⁺CD138⁺ engraftment are plotted. Percentages of donor cells reflect the percent of total CD45⁺ cells.

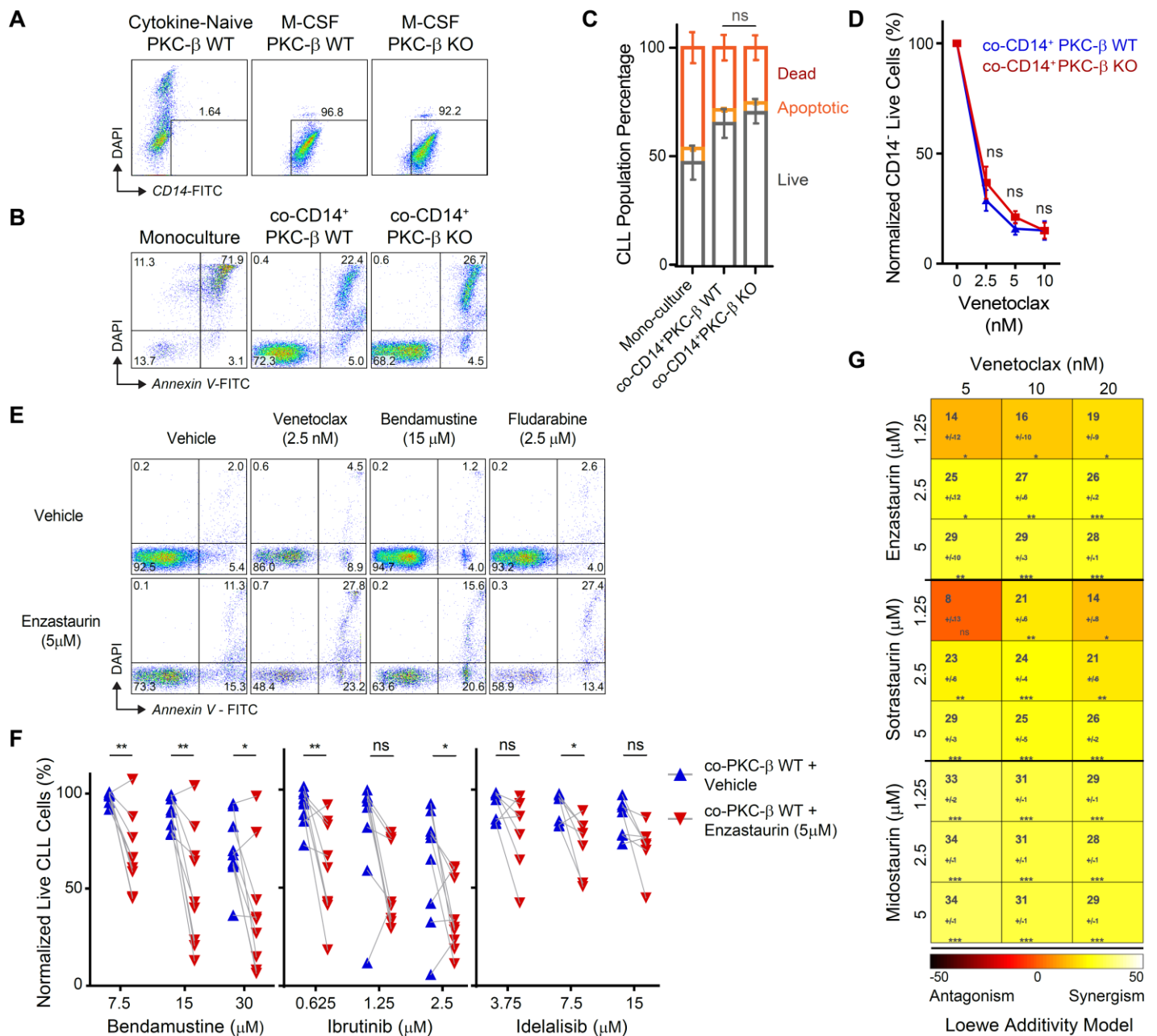


Fig. S4. Monocytes confer CLL survival support but not PKC- β dependent EMDR, in contrast to MSCs. (A) Representative flow cytometry plots of cytokine-naive PKC- β WT, and M-CSF cultured PKC- β WT and PKC- β KO stroma. (B) Representative Annexin-V and DAPI flow cytometry plots of mono-cultured or respective co-cultured CLL cells, 72 hours post-seeding of CLL. (C) Percentage of Live (Annexin-V⁻, DAPI⁺), Annexin-V⁺, and Dead (DAPI⁺Annexin-V⁺) stained cells are shown for individually co-cultured primary CLL (n=5 unique patients) for the three respective conditions. Statistical comparisons are shown for the live-cell fractions of each condition. (D) Viability of CLL cells following 72 hours of respective co-culture (CD14⁺ PKC- β WT or CD14⁺ PKC- β KO cells) with 48 hours of exposure to increasing doses of venetoclax (n=6). (E) Representative Annexin-V and DAPI flow cytometry plots of mono-cultured or respective co-cultured CLL cells, 72 hours post-seeding of CLL. (F) Viability of CLL cells following 72 hours of PKC- β WT co-culture with 48 hours of exposure to increasing doses of respective bendamustine (n=8), ibrutinib (n=9), or idelalisib (n=7) \pm enzastaurin treatment. Statistical significance was assessed using a paired two-tail Student-T-test. (G) Synergism was calculated using Combenefit Software (CRUK), within the Loewe additivity model, for venetoclax combined with enzastaurin, sotrastaurin, or midostaurin, respectively (n=6 per combination).

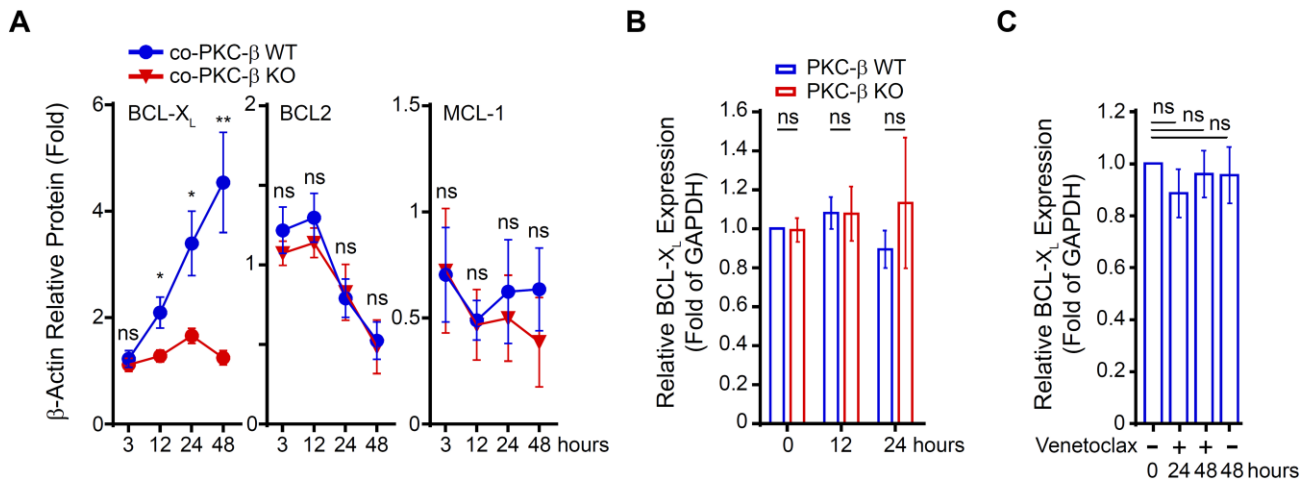


Fig. S5. PKC-β-mediated EMDR involves increased protein levels of BCL-X_L. (A) Graphs of respective BCL-X_L (n=5), BCL-2 (n=5), MCL-1 (n=3) fold protein levels in CLL cells co-cultured with either PKC-β WT or PKC-β KO, relative to β-Actin after indicated exposures to 2.5 nM venetoclax. (B) Quantitative-PCR measured relative BCL-X_L expression in CLL (n=4) in the respective presence of PKC-β WT or KO stromal co-culture ($2^{-\Delta\Delta CT}$). (C) Quantitative-PCR measured relative BCL-X_L expression in CLL (n=6) co-cultured with PKC-β WT ± venetoclax treatment (2.5 nM) for the indicated timepoints.

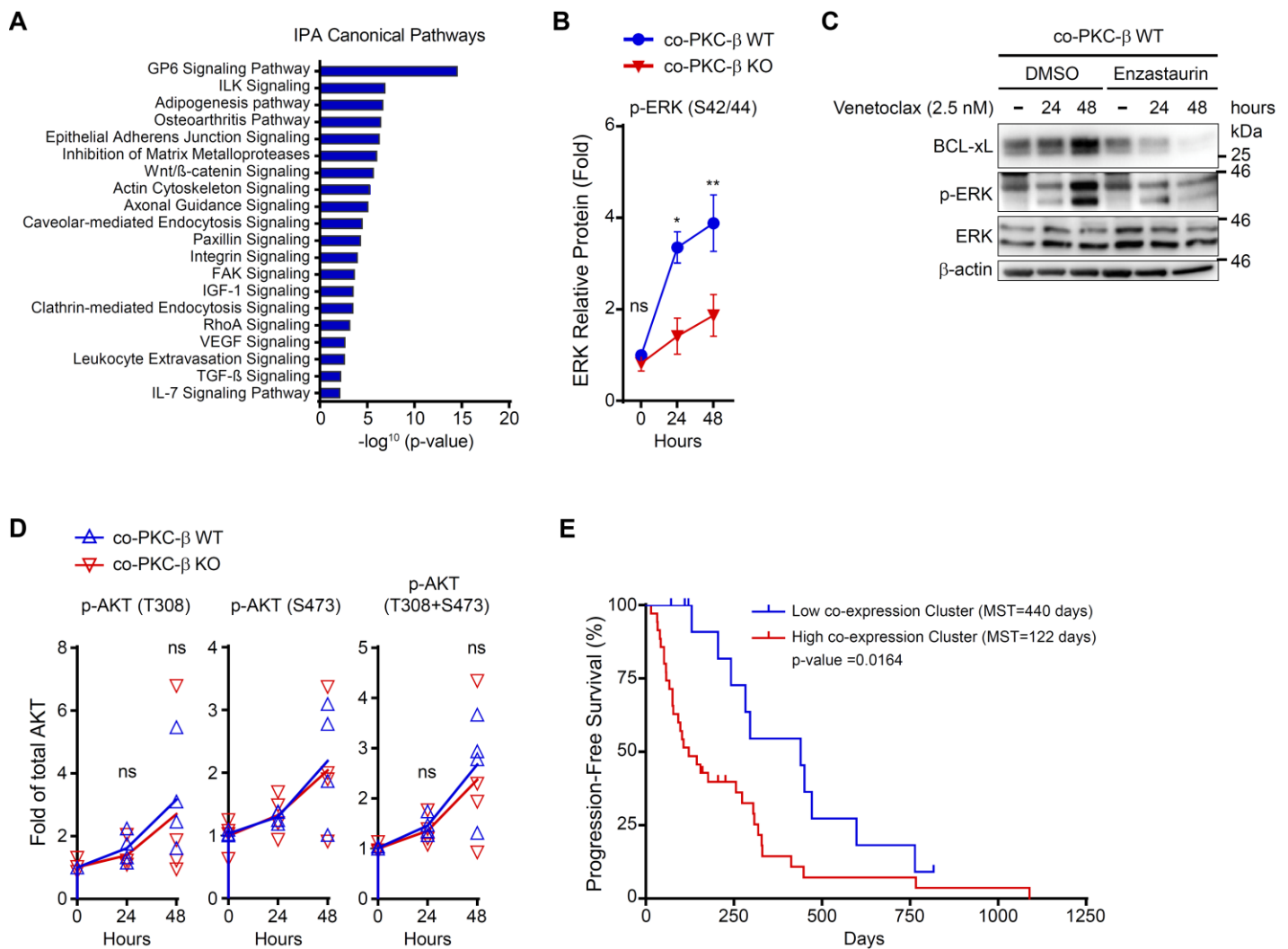


Fig. S6. CLL signaling pathways regulated by stromal PKC- β correlate with clinical outcomes. (A) IPA analysis of canonical pathways activated in CLL cells ($n=3$) co-cultured with PKC- β WT stroma compared to CLL cells co-cultured with PKC- β KO stroma ($n=3$), both in the presence of venetoclax (1.25 nM). (B) Graph of p-ERK ($n=4$) fold protein levels in CLL cells co-cultured with either PKC- β WT or PKC- β KO, relative to total ERK after indicated exposures to 2.5 nM venetoclax. (C) BCL-X_L, phosphorylated ERK (Thr202/Thr204), total ERK and β -actin immunoblots of primary CLL at indicated time-points of venetoclax treatment, co-cultured with PKC- β WT stroma \pm enzastaurin (5 μ M). (D, related to Fig. 3I) Graphs of respective phosphorylated-AKT relative fold protein levels in CLL cells co-cultured with either PKC- β WT or PKC- β KO after indicated exposures to 2.5 nM venetoclax. (E, related to Fig. 3K) Kaplan-Meier curves (x-axis with time since treatment) according to respective clusters ("High co-expression" vs. "Low co-expression"), showing statistically significant differences (pairwise log-rank tests) for median progression-free survival (PFS) ("High co-expression": 122 days vs "Low co-expression": 440 days; $p < 0.02$).

(E) *In vitro* downregulation of Vcam1 in PKC- β WT stroma co-cultured with CLL \pm increasing concentrations of enzastaurin. **(F, related to Fig. 5H)** Graph of CD106 (Vcam1) MFIs from mono-cultured PKC- β WT stroma with Crispr-deleted cells transduced with sgRNA control (n=3) or *Tfeb*-deleted stroma using 4 unique sgRNAs, respectively (n=8 total values; duplicate measurements for n=4 sgRNAs).

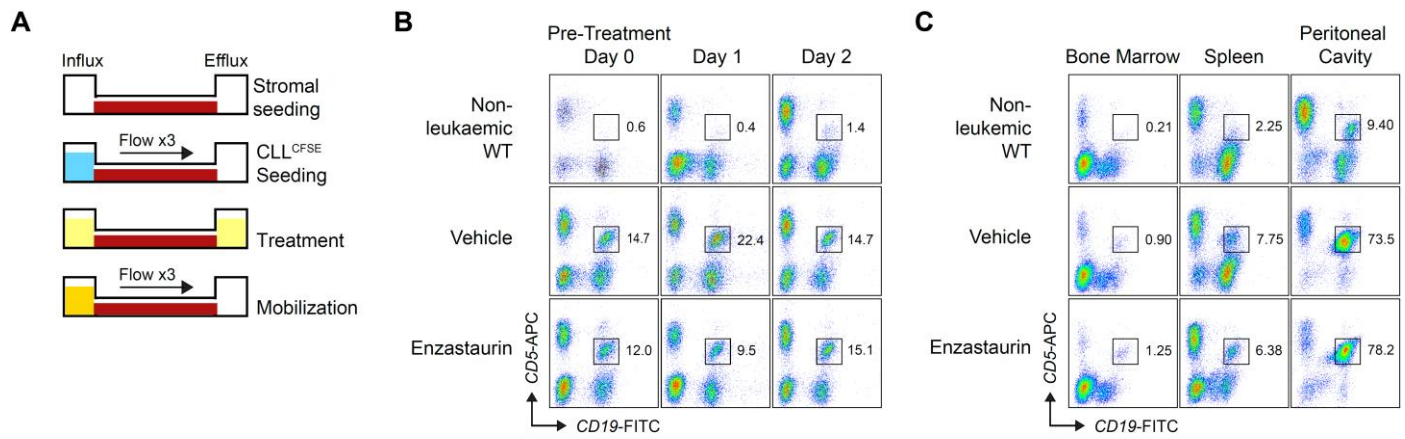


Fig. S8. PKC- β is dispensable for *in vitro* and *in vivo* mobilization of leukemia. (A) Schematic of adhesion and mobilization assays utilizing channel slides. **(B, related to Fig. 5K)** Representative flow cytometry plots of CD19⁺CD5⁺ cells in the peripheral blood before and during treatment with enzastaurin or vehicle, respectively. **(C, related to Fig. 5L)** Representative flow cytometry plots of CD19⁺CD5⁺ cells in the bone marrow, spleen, and peritoneal cavity after treatment with enzastaurin or vehicle, respectively.

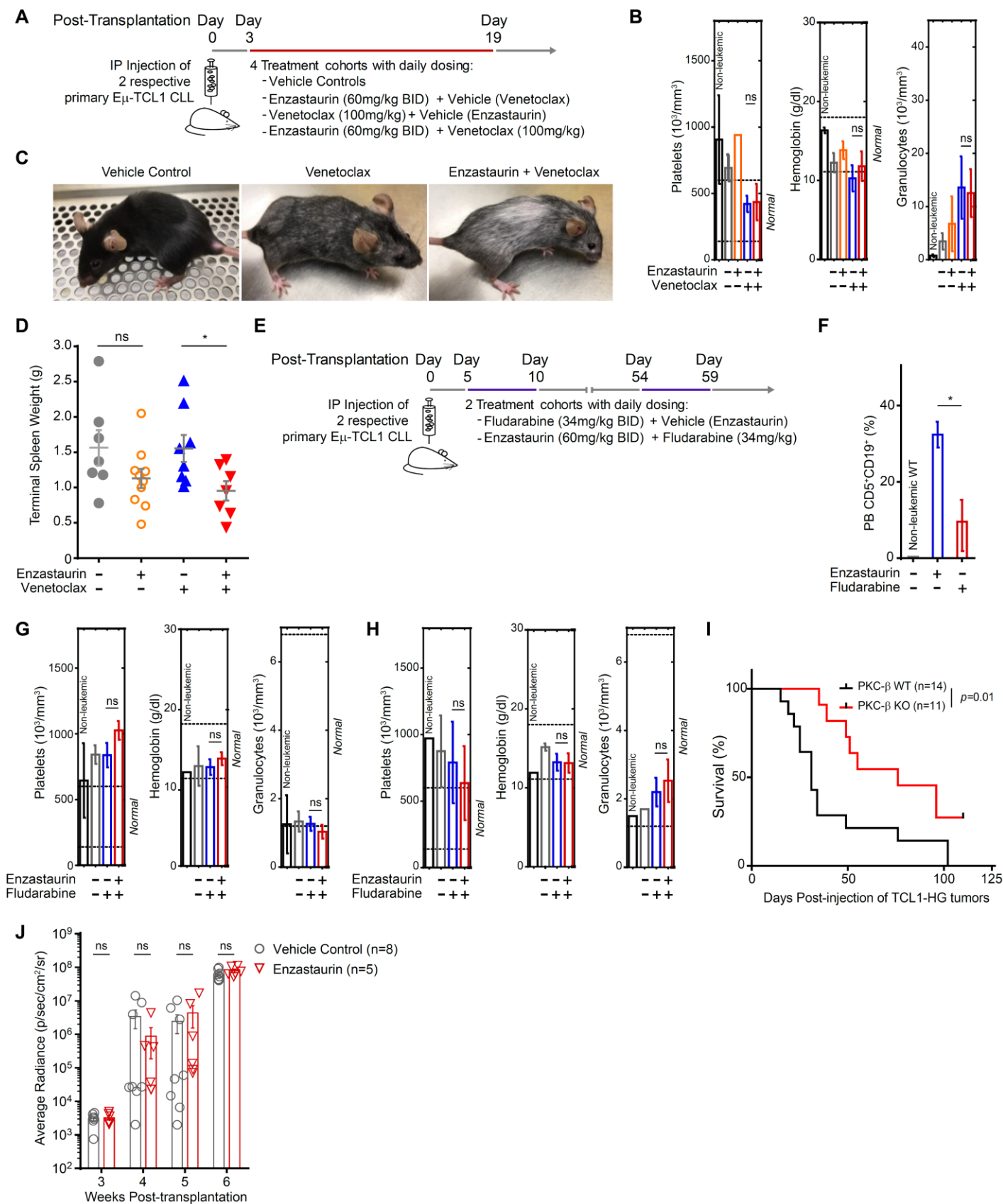


Fig. S9. *In vivo* co-targeting of PKC- β does not contribute to increased off-target cytotoxicity. (A) *In vivo* treatment schematic of E μ -TCL1 CLL model using venetoclax, enzastaurin, mock control or venetoclax + enzastaurin. (B)

Complete blood counts (CBC) of non-leukemic WT control (n=2), vehicle control (n=4), enzastaurin-treated (n=4), venetoclax-treated (n=4), and enzastaurin + venetoclax treated (n=4) mice on Day 32 post-end of treatment. Normal blood counts are indicated between dashed lines. Statistical differences were calculated by unpaired Student T-Test. **(C)** Photographs at week 12 post-treatment of representative mice from vehicle, venetoclax, and enzastaurin + venetoclax treatment cohorts. **(D)** Terminal spleen weights for individuals of indicated treatment cohorts. **(E)** Schematic of *in vivo* treatment model of E μ -TCL1 CLL using fludarabine + vehicle or fludarabine + enzastaurin. **(F)** Percentage of detectable peripheral blood CD5⁺CD19⁺ cells in non-leukemic controls (n=3), fludarabine-treated (n=3) and fludarabine + enzastaurin treated mice (n=4), on days 25 - 28 post-end of first treatment cycle. **(G)** Complete blood counts of non-leukemic WT control (n=2), vehicle control (n=3), fludarabine-treated (n=3), and enzastaurin + fludarabine treated (n=3) mice on Day 16 post-end of first-treatment cycle. **(H)** Complete blood counts of non-leukemic WT control (n=1), vehicle control (n=2), fludarabine-treated (n=3), and enzastaurin + fludarabine-treated (n=3) mice on Day 10 post-end of second-treatment cycle. **(I)** TCL1-HG cells were transplanted into either PKC- β WT (MST= 31 days) or PKC- β KO recipients (MST= 76 days). **(J)** Average radiance obtained by bioluminescent imaging of ALL-PDX engrafted NSG animals treated with either vehicle control or enzastaurin. Statistical significance was determined using an unpaired two-tail Student T-test.

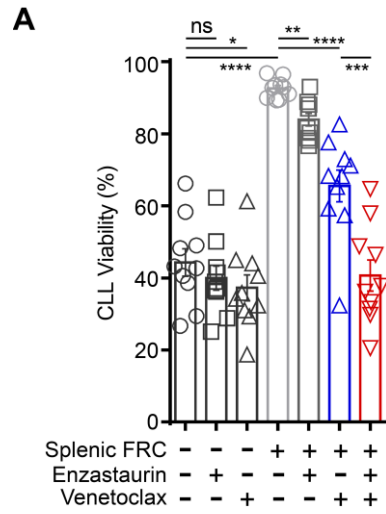


Fig. S10. EMDR derived from splenic stroma is mitigated by PKC- β antagonism. (A) *In vitro* treatment of primary CLL (n=10) in monoculture or co-culture on splenic FRC stroma (gp38⁺CD31⁺) treated with either vehicle control, enzastaurin, venetoclax, or venetoclax + enzastaurin. Statistical significance was determined using a paired two-tail Student T-test.

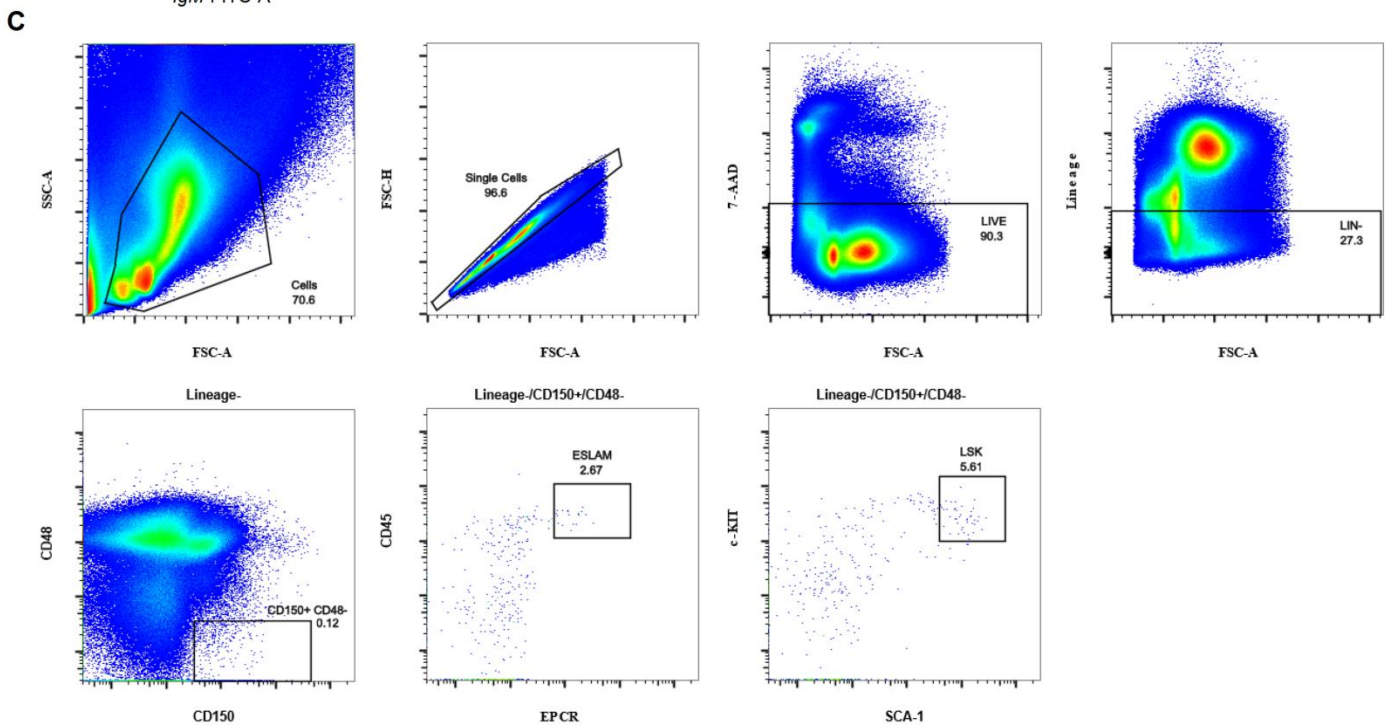
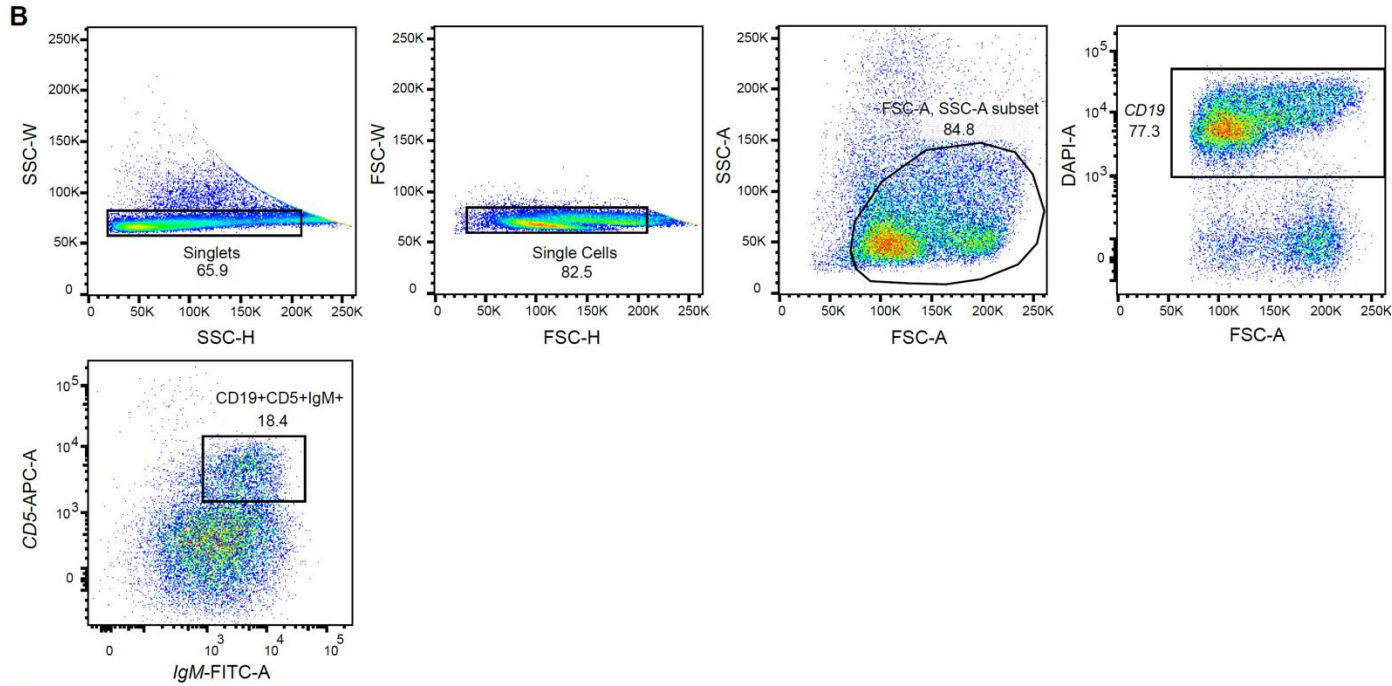
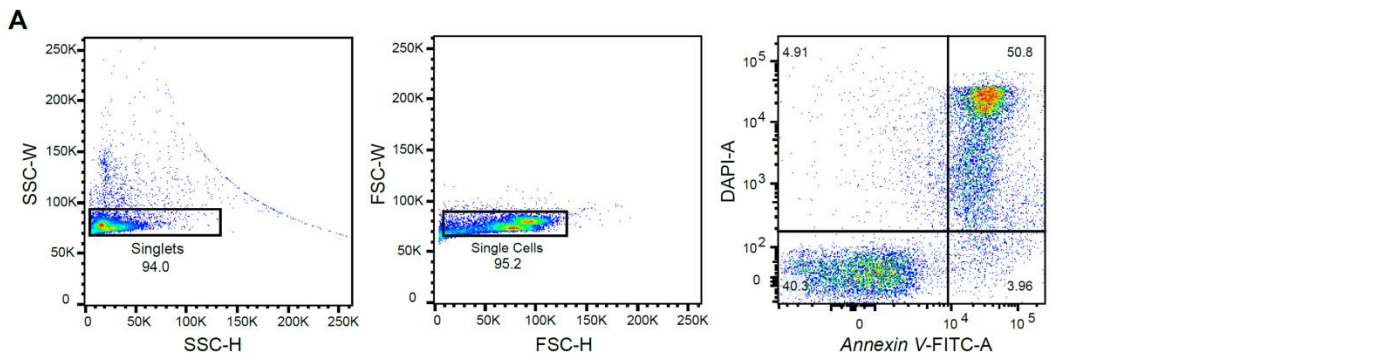


Fig. S11. Representative FACS gating strategies. (A) Representative FACS gating for co-culture in vitro cytotoxicity assays (left to right). **(B)** FACS gating strategy for immunophenotyping of peritoneal cells from chimeric mice (left to right, per row). **(C)** Representative FACS gating strategy for in vivo HSC phenotyping (left to right, per row).

Supplemental Table S1: Patient characteristics

Chronic lymphocytic leukemia (Figures 2-5,S4-S7,S9-S11)			
Encrypted Patient ID	Cytogenetic results/ IGVH-status*	Live cell decrease w/enzastaurin + venetoclax (5 nM) vs. venetoclax alone	Live cell decrease w/enzastaurin +fludarabine (2.5 uM) vs. fludarabine alone
BP0401	Del13q14, M-IGVH	57.9%	40.8%
BS4072	Del13q14, UM-IGVH	-0.8%	37.9%
CL9959	Data not available	45.8%	28.5%
DP3335	Del13q14, M-IGVH	48.4%	19.2%
KA9559	Negative FISH panel	26.4%	14.2%
DI7353	Del13q	55.7%	-1.9%
BF59	Del13q, Del17p	51.3%	-3.7%
JC2614	Normal FISH panel, UM-IGVH	69.4%	5.8%
SJ35	Data not available	80.8%	25.1%
MB6377	Del17p	23.8%	24.4%
MO2147	P53 mutated	41.9%	56.5%
EB5492	Trisomy12	14.7%	2.3%
CH8051	Del17p	33.4%	-1.9%
EG5792	Trisomy12	25.6%	18.9%
AR30	Del13q, Del11q	27.4%	16.8%
AS5041	Del13q, Del17p, Del11q	40.4%	-3.1%
JC833	Del13q, Del11p	16.7%	21.8%
SM7753	Del13q, Del17p, Trisomy12	27.2%	-3.8%
PF8841	Del17p, Trisomy13q14	37.5%	37.0%
DW5916	Trisomy 12	19.1%	13.0%
Mantle Cell Lymphoma (Figure 6F)			
Encrypted Patient ID	Cytogenetic results/ IHC/FC	Live cell decrease w/enzastaurin + venetoclax (2.5 nM) vs. venetoclax alone	Live cell decrease w/enzastaurin + venetoclax (5 nM) vs. venetoclax alone
12414	t(11;14), Cyclin D1+	19.6%	25.8%
10084	t(11;14), Cyclin D1+	40.4%	34.0%
12267	t(11;14), Cyclin D1+	40.9%	46.8%
FC0175	CD19 ⁺ , CD20 ⁺ , CD79b ⁺ CD5 ⁺ , CD200 ⁻ (FISH unavailable)	43.9%	41.7%
PG220	Data not available	47.1%	38.9%
V314	Blastoid MCL, Cyclin D1+	3.8%	1.8%
V323	t(11;14), monosomy 12 Cyclin D1+, p53 Del	39.2%	27.1%
M13	CD5+, PAX5+, FCM7++	9.5%	6.8%
B-Acute lymphoblastic leukemia (Figure 6G,H)			
Encrypted Patient ID	Cytogenetic results	Live cell decrease w/enzastaurin + dexamethasone (0.1 nM) vs. dexamethasone alone	Live cell decrease w/enzastaurin + vincristine (50 nM) vs. vincristine alone
190615A	Complex Karyotype	81.4%	57.8%
310315A	MLL-AF9	-	47.1%
201115A	TEL-AML1	15.3%	39.7%
260416A	TEL-AML1	76.3%	33.5%
261215A	TEL-AML1	70.0%	42.6%
170815A	E2A-PBX1	41.3%	34.9%
080915A	Hyperdyploid	18.4%	13.3%
130516A	TEL-AML1	15.0%	43.3%
131015A	High-Hyperdyploid	56.6%	13.3%
170816A	High-Hyperdyploid	21.1%	11.4%

* UM/MIGVH=unmutated/ mutated IGVH
IHC=immunohistochemistry
FC=flow cytometry

Supplemental Table S2: Key resources

Antibodies	Source	Catalog #
Anti-Human FcR (1:200 dilution)	Biologend	422302
Anti- Mouse FcR (1:200 dilution)	Biologend	101320
Anti-Mouse CD45.1 (A20)-FITC (1:200 dilution)	Tonbo Bioscience	35-0453-U500
Anti-Mouse CD45.2 (104)-APC (1:200 dilution)	Biologend	109814
Anti-Mouse CD45.1 - PerCP/Cy5.5 (1:200 dilution)	Biologend	110728
Anti-Human CD19 - APC (1:200 dilution)	Biologend	302212
Anti-IgM-FITC (1:200 dilution)	Biologend	406506
Anti-Mouse CD138-BV421 (1:200 dilution)	Biologend	142523
Anti-Mouse CD19-BV421 (1:200 dilution)	Biologend	302233
Anti-Mouse CD5-APC (1:200 dilution)	Biologend	100626
Anti-Mouse CD19-FITC (1:200 dilution)	Biologend	101505
Anti-Mouse CD19-APC (1:200 dilution)	Biologend	115112
Anti-Mouse CD106-APC (1:200 dilution)	Biologend	105717
Anti-Mouse B220-BV421 (RA3-6B2) (1:100 dilution)	Biologend	103239
Anti-Mouse CD24-BV605 (MI/69) (1:100 dilution)	Biologend	101827
Anti-Mouse IgD-FITC (11-26c.2a) (1:100 dilution)	Biologend	405704
Anti-Mouse CD43-APC (S7) (1:100 dilution)	Becton Dickinson Biosciences	560663
Anti-Mouse CD249-PE(6C3) (1:100 dilution)	eBioscience	12-5891-81
Anti-Mouse IgM-PerCPe710 (II/41) (1:100 dilution)	eBioscience	46-5790-82
Anti-Mouse Ter119-PeCy7 (1:200 dilution)	Becton Dickinson Biosciences	557853
Anti-Mouse CD45-PeCy7 (1:400 dilution)	eBioscience	25-0451-82
Anti-Mouse CD31-APC (1:100 dilution)	Becton Dickinson Biosciences	551262
Anti-Mouse CD51-BV (1:100 dilution)	Becton Dickinson Biosciences	740062
Anti-Mouse Sca-1-APCCy7 (1:100 dilution)	Becton Dickinson Biosciences	560654
Anti-Mouse CD14-FITC (1:200 dilution)	Biologend	123311
Anti-Mouse/Human CD45R/B220-FITC (1:200 dilution)	Biologend	103206
Anti-Human CD5-FITC (1:100 dilution)	Becton Dickinson Biosciences	555352
Anti-Human CD19-APC (1:100 dilution)	Becton Dickinson Biosciences	555415
Anti-Human CD19-BV421(HIB19) (1:100 dilution)	Biologend	302233
Anti-Human TFEB (1:500 dilution)	Cell Signaling Technology	37785S
Anti-Human TBP (1:1000 dilution)	Cell Signaling Technology	8515S
Anti-Human BCL-XL (1:1000 dilution)	Cell Signaling Technology	54H6
Anti-Human BCL-2 (1:1000 dilution)	Becton Dickinson Biosciences	610539
Anti-Human MCL-1 (1:500 dilution)	Santa Cruz Biotech	SC-819
Anti-Human BCL-2A1 (1:1000 dilution)	Sigma-Aldrich	AV09047
Anti-Human NOXA (1:500 dilution)	Abcam	ab140129
Anti-Human PUMA (1:500 dilution)	Abcam	ab33906
Anti-Human BIM (1:500 dilution)	Becton Dickinson Biosciences	559685
Anti-Human p-ERK (1:1000 dilution)	Cell Signaling Technology	4370s
Anti-Human ERK (1:1000 dilution)	Cell Signaling Technology	9102s
Anti-Human p-JNK (1:1000 dilution)	Cell Signaling Technology	9251s
Anti-Human p-p38MAPK (1:1000 dilution)	Cell Signaling Technology	9211s
Anti-Human LAMP1 (1:1000 dilution)	Cell Signaling Technology	9091s
P-p42/44 MAPK (1:500 dilution)	Cell Signaling Technology	9101s
Anti-β-Actin (1:5000 dilution)	Sigma-Aldrich	A5441-.2ML
Anti-Mouse Lamp1-PE (1D4B) (1:100 dilution)	Santa Cruz Biotech	sc-19992-PE
Anti-Mouse Lamp2-Alexa488 (M3/84) (1:100 dilution)	Biologend	108510

Biological Samples	Source	Catalog #
CLL Patient Samples (Project ID: 07/MRE05/44)	Cambridge University Hospitals - Addenbrookes	N/A
MCL Patient Samples (Project ID: 1894/07)	Technical University Munich	N/A
Patient-derived xenografts (Erasmus IRB)	University College London	N/A
Murine stromal cells	This paper	N/A
Chemical Compounds	Source	Catalog #
Zombie Aqua - BV510 (1:2000 dilution)	Biologend	423101
Annexin-V FITC (1:50 dilution)	Biologend	640945
DAPI (3 μ M)	Biologend	422801
Enzastaurin	Sigma-Aldrich	SML0762
Sotrastaurin	Selleck Chemicals	S2791
Bendamustine	Selleck Chemicals	S1212
Idelalisib	Selleck Chemicals	S2226
Midostaurin	Selleck Chemicals	S8064
Venetoclax	LC Labs	v-3579
Fludarabine	Cayman Chemicals	14128
Ibrutinib	SYNKinase	SYN-1171
Dexamethasone	Sigma-Aldrich	D4902
Vincristine Sulfate	Sigma-Aldrich	V8879
Critical Commercial Assays	Source	Catalog #
LEGENDplex Mouse Immunoglobulin Isotyping Panel	Biologend	740492

REFERENCES

60. L. Wang, S. Wang, W. Li, RSeQC: quality control of RNA-seq experiments, *Bioinformatics* **28**, 2184–2185 (2012).
61. A. Dobin, C. A. Davis, F. Schlesinger, J. Drenkow, C. Zaleski, S. Jha, P. Batut, M. Chaisson, T. R. Gingeras, STAR: ultrafast universal RNA-seq aligner, *Bioinformatics* **29**, 15–21 (2013).
62. S. Anders, P. T. Pyl, W. Huber, HTSeq--a Python framework to work with high-throughput sequencing data, *Bioinformatics* **31**, 166–169 (2015).
63. M. I. Love, W. Huber, S. Anders, Moderated estimation of fold change and dispersion for RNA-seq data with DESeq2, *Genome Biol.* **15**, 550 (2014).
64. A. Sturn, J. Quackenbush, Z. Trajanoski, Genesis: cluster analysis of microarray data, *Bioinformatics* **18**, 207–208 (2002).
65. M. P. Weekes, S. Y. L. Tan, E. Poole, S. Talbot, R. Antrobus, D. L. Smith, C. Montag, S. P. Gygi, J. H. Sinclair, P. J. Lehner, Latency-associated degradation of the MRP1 drug transporter during latent human cytomegalovirus infection, *Science* **340**, 199–202 (2013).
66. E. J. Greenwood, N. J. Matheson, K. Wals, D. J. van den Boomen, R. Antrobus, J. C. Williamson, P. J. Lehner, Temporal proteomic analysis of HIV infection reveals remodelling of the host phosphoproteome by lentiviral Vif variants, *Elife* **5**, 12112 (2016).
67. R. Pan, L. J. Hogdal, J. M. Benito, D. Bucci, L. Han, G. Borthakur, J. Cortes, D. J. DeAngelo, L. Debose, H. Mu, H. Döhner, V. I. Gaidzik, I. Galinsky, L. S. Golfman, T. Haferlach, K. G. Harutyunyan, J. Hu, J. D. Levenson, G. Marcucci, M. Müschen, R. Newman, E. Park, P. P. Ruvolo, V. Ruvolo, J. Ryan, S. Schindela, P. Zweidler-McKay, R. M. Stone, H. Kantarjian, M. Andreeff, M. Konopleva, A. G. Letai, Selective BCL-2 inhibition by ABT-199 causes on-target cell death in acute myeloid leukemia, *Cancer Discov* **4**, 362–375 (2014).
68. N. L. M. Liem, R. A. Papa, C. G. Milross, M. A. Schmid, M. Tajbakhsh, S. Choi, C. D. Ramirez, A. M. Rice, M. Haber, M. D. Norris, K. L. MacKenzie, R. B. Lock, Characterization of childhood acute lymphoblastic leukemia xenograft models for the preclinical evaluation of new therapies, *Blood* **103**, 3905–3914 (2004).

DATA AVAILABILITY

The authors declare that the data supporting the findings of this study are available within the paper and its supplementary information.

The gene expression profile data have been deposited in the GEO database under accession numbers GSE119808 (CLL RNA-Seq, Figure 3) and GSE119813 (Stromal RNA-seq, Figure 4).

<https://www.ncbi.nlm.nih.gov/geo/query/acc.cgi?acc=GSE119808>

<https://www.ncbi.nlm.nih.gov/geo/query/acc.cgi?acc=GSE119813>

The mass spectrometry proteomics data have been deposited to the ProteomeXchange Consortium via the PRIDE partner repository with the dataset identifier PXD011062 and 10.6019/PXD011062.

<https://www.ebi.ac.uk/pride/archive/projects/PXD011062>

All other remaining data are available within the Article and Supplementary Files, or available from the authors upon request.